mathematics

MDPI

Article

An Improved Mathematical Theory for Designing Membrane Deflection-Based Rain Gauges

Jun-Yi Sun [1,2,*], Ning Li [1] and Xiao-Ting He [1,2]

[1] School of Civil Engineering, Chongqing University, Chongqing 400045, China; 202116131316@cqu.edu.cn (N.L.); hexiaoting@cqu.edu.cn (X.-T.H.)
[2] Key Laboratory of New Technology for Construction of Cities in Mountain Area (Chongqing University), Ministry of Education, Chongqing 400045, China
* Correspondence: sunjunyi@cqu.edu.cn; Tel.: +86-023-65120720

Abstract: This paper is devoted to developing a more refined mathematical theory for designing the previously proposed membrane deflection-based rain gauges. The differential-integral equations governing the large deflection behavior of the membrane are improved by modifying the geometric equations, and more accurate power-series solutions of the large deflection problem are provided, resulting in a new and more refined mathematical theory for designing such rain gauges. Examples are presented to illustrate how to analyze the convergence of the power-series solutions and how to numerically calibrate membrane deflection-based linear rain gauges. In addition, some important issues are demonstrated, analyzed, and discussed, such as the superiority of the new mathematical theory over the old one, the reason why the classical geometric equations cause errors, and the influence of changing design parameters on the input–output relationships of rain gauges.

Keywords: conductive membrane; transversely loading; axisymmetric deformation; large deflection; power-series solution

MSC: 74G10; 74K15

check for updates

Citation: Sun, J.-Y.; Li, N.; He, X.-T. An Improved Mathematical Theory for Designing Membrane Deflection-Based Rain Gauges. *Mathematics* **2023**, *11*, 3438. https://doi.org/10.3390/math11163438

Academic Editor: Pedro Navas

Received: 29 June 2023
Revised: 30 July 2023
Accepted: 4 August 2023
Published: 8 August 2023

Copyright: © 2023 by the authors. Licensee MDPI, Basel, Switzerland. This article is an open access article distributed under the terms and conditions of the Creative Commons Attribution (CC BY) license (https://creativecommons.org/licenses/by/4.0/).

1. Introduction

Many thin films are able to exhibit large elastic deflections when subjected to external loads [1–6], which makes it possible to develop devices or instruments based on film deflection [7–12]. In our previous study [13], to overcome the shortcomings of the existing rain gauges, a new type of membrane deflection-based rain gauge was proposed, which involves a liquid–structure interaction of a peripherally fixed circular membrane under liquid weight loading. Such a fluid–solid coupling problem presents serious analytical difficulties, which involves the analytical solution to differential-integral governing equations. The mathematical theory for designing such rain gauges, which is presented in our previous study [13], is observed to be inaccurate. It is suitable only for the design of nonlinear (rather than linear) rain gauges, because the ranges of the nearly-linear (seemingly following a linear-dependent relationship) segments in the nonlinear input–output relationships of the rain gauges, which it can provide, are too small or too narrow. The main purpose of this study is to present a new and more accurate mathematical theory suitable for the design of both nonlinear and linear rain gauges.

The precipitation sensors are generally divided into three major standard categories: manual rain gauges, tipping-bucket rain gauges [14–18], and weighing rain gauges [19,20], in addition to novel optical infrared sensors [21–23]. Among them, the most popular are the tipping-bucket rain gauges, as they are simple, robust, suitable for different data loggers, and provide an available point measurement, especially suitable for installation in remote areas. Applications of tipping-bucket gauges (also including weighing rain gauges) usually presuppose the static or dynamic calibrations in the laboratory and in the field [24–27],

and although very troublesome, they are necessary to do, otherwise, the measurements of precipitation will be accompanied by errors [28–31]. In general, due to various factors, such as calibration errors, the measurements of precipitation may be underestimated by 5% to 40% [32]. In our previous study [13], we proposed developing a new type of rain gauge using the elastic deflection of conductive membranes, namely the membrane elastic deflection-based rain gauge. As opposed to tipping-bucket or weighing rain gauges, this new type of rain gauge does not require performing the calibration for volumetric metering of rainwater, thus avoiding the measurement errors of precipitation caused by this.

The basic configuration and working principle of a membrane deflection-based rain gauge are shown in Figure 1. The rainwater is collected by the rainwater collector funnel that is placed outside. The area of the upward opening of the rainwater collector funnel will be used to determine the amount of rainfall per unit area. The conductive circular membrane is used as the upper electrode plate of capacitors and is fixed to the wall of the circular tank when it is initially flat, resulting in the circular rainwater-collecting tank. The collected rainwater flows into the circular rainwater-collecting tank from the rainwater collector funnel, resulting in the deflection of the conductive circular membrane. Therefore, the upper electrode plate is called a movable electrode plate due to the membrane deflection, while the lower electrode plate, thickly coated with the insulator layer, which is made of a conductive circular thin plate, is an unmovable electrode plate because it is fixed on the substrate. The non-parallel plate variable capacitor between the upper and lower electrode plates is made of two capacitors in series: one is the non-parallel plate variable capacitor between the movable upper electrode plate and the insulator layer, and the other is the parallel plate fixed capacitor between the insulator layer and the unmovable lower electrode plate. The dielectric material between the upper electrode plate and the insulator layer is air, and a small hole is opened in the wall of the circular tank to allow air to pass through, which is located between the upper electrode plate and the insulator layer (see Figure 1).

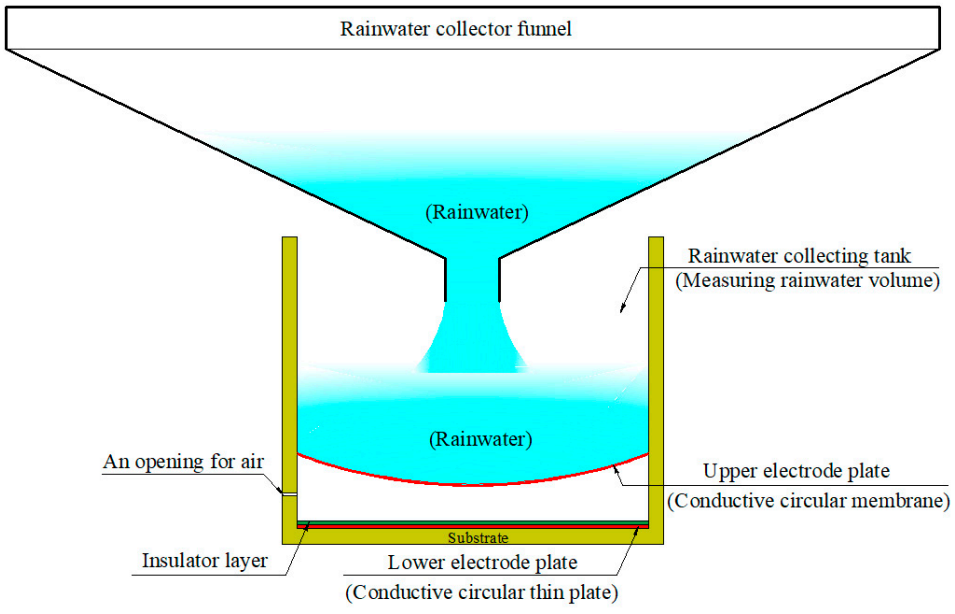

Figure 1. The configuration and working principle of a membrane deflection-based rain gauge.

Obviously, the collected rainwater in the circular rainwater-collecting tank, as an external load acting on the conductive circular membrane, causes the elastic deflection of the conductive circular membrane, determines the spatial geometry of the movable upper electrode plate (i.e., the deflected conductive circular membrane), and thus, determines the capacitance of the non-parallel plate variable capacitor between the movable upper electrode plate and the insulator layer. Therefore, if the magnitude of the external loads acting on the conductive circular membrane is defined by the volume of the collected

rainwater in the circular rainwater-collecting tank, then, once the elastic behavior of the conductive circular membrane under the external loads is analytically solved, the volume of the collected rainwater in the circular rainwater-collecting tank can be determined by using the deflection analytical solution. At the same time, the spatial geometry of the deflected conductive circular membrane (i.e., the movable upper electrode plate) can also be determined by using the deflection analytical solution; that is, the capacitance of the non-parallel plate variable capacitor between the movable upper electrode plate and the insulator layer can be determined by using the deflection analytical solution. On the other hand, the capacitance of the parallel plate fixed capacitor between the insulator layer and the unmovable lower electrode plate is constant and, for given design parameters, can be determined by calculation. Therefore, the total capacitance of the non-parallel plate variable capacitor between the upper and lower electrode plates, which can be determined by measurements, is in one-to-one correspondence with the volume of the collected rainwater in the circular rainwater-collecting tank. In other words, the volume of the collected rainwater in the circular rainwater-collecting tank can be determined by measuring the total capacitance of the non-parallel plate variable capacitor between the upper and lower electrode plates. Usually, it is customary to express the rainfall in terms of the height of rainfall per unit area per unit time. Therefore, since any two capacitance measurements will result in two values of volume of the collected rainwater in the circular rainwater-collecting tank, the height of rainfall per unit area per unit time can finally be determined by the volume difference between the two measurements divided by the upward opening area of the rainwater collector funnel, and by the time difference between the two measurements.

However, it can be seen from Figure 1 that there is an interaction between the applied rainwater loads and the deflected conductive circular membrane. The rainwater applied to the conductive circular membrane, as an external load acting on the membrane, gives rise to the deflection of the membrane. In turn, the deflection change gives rise to the distribution change of the rainwater on the conductive circular membrane, i.e., the change in the external loads acting on the membrane. In other words, the liquid action causes the solid response, and in turn, the solid response changes the liquid action, which is commonly referred to as the fluid–solid coupling or interaction problem. Previous studies have shown that the elastic behavior of the conductive circular membrane can be described or governed by a set of differential-integral equations, and the size of membrane deflections has a great influence on the accuracy of the established governing equations [33–35]. In general, it is sufficient to formulate governing equations with lower precision for small deflection problems, because high-precision governing equations will bring difficulties to the subsequent analytical solution. However, if the governing equations with low precision are used for large deflection problems, errors are inevitable. The governing equations used in [13] are the governing equations with low precision, and therefore, only apply to small deflection problems, not to large deflection problems. However, the elastic deflection exhibited by the conductive circular membrane in Figure 1 may reach half of the radius of the circular membrane; therefore, the governing equations used in [13] are practically inapplicable in this case. Therefore, it is recommended that the mathematical theory for designing membrane deflection-based rain gauges, presented in [13], should not be used to avoid causing errors.

In this paper, the differential-integral equations governing the large deflection behavior of the conductive circular membrane are improved by modifying the geometric equations, and more accurate power-series solutions of the large deflection problem are presented, resulting in a new and more refined mathematical theory for designing membrane deflection-based rain gauges. The remainder of this paper is organized as follows. In the following section, the liquid–structure coupling problem in Figure 1: the large deflection problem of the peripherally fixed conductive circular membrane under liquid weight loading, is reformulated, the power-series method for differential equations is used to analytically solve the resulting differential-integral governing equations, and examples are

presented to illustrate how to numerically analyze the convergence of the resulting power-series solutions. In Section 3, the analytical relationships between the input capacitance and the output rainwater volume are derived. Examples are provided to illustrate how to numerically calculate the nonlinear input–output relationships of the membrane deflection-based linear rain gauges, and the clear differences between the numerical results calculated by using the new and old mathematical theories are graphically shown. Then, an example is presented to illustrate how to numerically calibrate a membrane deflection-based linear rain gauge. In Section 4, some important issues are analyzed and discussed, such as the reason why the classical geometric equations cause errors, and the influence of changing design parameters on the input–output relationships of membrane deflection-based rain gauges. The concluding remarks are presented in Section 5.

2. Governing Equations and Power-Series Solutions

2.1. Governing Equations

Suppose that an initially flat, conductive, circular membrane with radius a, thickness h, Poisson's ratio ν, and Young's modulus of elasticity E is fixed peripherally at the inner wall of the rainwater-collecting tank, as shown in Figure 1, and then it is deflected toward the insulator layer due to the action of the collected rainwater in the rainwater-collecting tank; that is, the action of the so-called liquid weight loading, denoted by $q(r)$, where the height of the rainwater above the plane in which the initially flat, peripherally fixed, conductive, circular membrane is located is denoted by H. A free body is taken from the central portion of the deflected circular membrane in Figure 1, whose radius is $0 \leq r \leq a$, to study its static problem of equilibrium, as shown in Figure 2, where the origin, o, of the introduced cylindrical coordinate system (r, φ, w) is placed in the centroid of the initially flat circular membrane. The dash-dotted line represents the geometric middle plane of the initially flat circular membrane in which the polar coordinate plane (r, φ) is located, r, φ, and w are the radial, circumferential, and transverse coordinates, respectively, w also denotes the transverse displacement of the deflected circular membrane under the action of the loads, $q(r)$, σ_r denotes the radial stress, and θ denotes the slope angle at a point on the geometric middle plane of the deflected circular membrane.

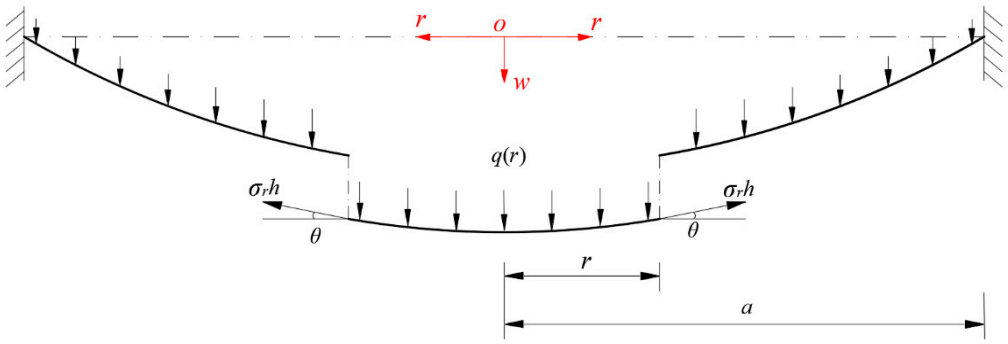

Figure 2. Sketch of a free body with radius $0 \leq r \leq a$.

In particular, it is noted that the external loads, $q(r)$, acting on the conductive circular membrane should include the actions of two parts of rainwater: one is the rainwater with the height H above the polar plane (r, φ), and the other is the rainwater with the height $w(r)$ below the polar plane (r, φ). At point r, the total height of the collected rainwater is equal to H plus $w(r)$.

The out-of-plane equilibrium equation can be derived as follows. The external force $F(r)$ acting on the free body, no matter how the circular membrane is deflected, is always downward, and is given by

$$F(r) = \int_0^r q(r)\mathrm{d}r = \rho\, g \int_0^r [H + w(r)] \cdot 2\pi r \mathrm{d}r = \rho\, g \pi r^2 H + 2\pi\rho\, g \int_0^r w(r) r \mathrm{d}r. \quad (1)$$

The upward force is only the component of the membrane force $\sigma_r h$ acting on the boundary r. Therefore, the out-of-plane equilibrium condition, when the resultant force in the vertical direction is equal to zero, yields

$$2\pi r\sigma_r h \sin\theta = F(r) = \rho\, g\pi r^2 H + 2\pi\rho\, g\int_0^r w(r)r\mathrm{d}r, \tag{2}$$

where

$$\sin\theta = 1/\sqrt{1+1/\tan^2\theta} = 1/\sqrt{1+1/(-\mathrm{d}w/\mathrm{d}r)^2}. \tag{3}$$

After substituting Equation (3) into Equation (2), the out-of-plane equilibrium equation may finally be written as

$$\frac{2r\sigma_r h}{\sqrt{1+1/(-\mathrm{d}w/\mathrm{d}r)^2}} = \rho g r^2 H + 2\rho g\int_0^r w(r)r\mathrm{d}r. \tag{4}$$

The in-plane equilibrium equation is [13]

$$\frac{\mathrm{d}}{\mathrm{d}r}(r\sigma_r) - \sigma_t = 0, \tag{5}$$

where σ_t denotes the circumferential stress.

The classic geometric equations used in [13] do not fully consider the contribution of deflection to the geometric relationship between radial strain and radial displacement. The classical geometric equations have been improved in [34]. If the radial and circumferential strains are denoted by e_r and e_t, and the radial displacement is denoted by u, then the improved geometric equations may be written as

$$e_r = [(1+\frac{\mathrm{d}u}{\mathrm{d}r})^2 + (\frac{\mathrm{d}w}{\mathrm{d}r})^2]^{1/2} - 1 \tag{6}$$

and

$$e_t = \frac{u}{r}. \tag{7}$$

By comparing Equation (6) here with Equation (6) presented in [13], it can be seen that the radial geometric equation here more fully considers the contribution of deflection to the geometric relationship between radial strain and radial displacement.

In addition, the physical equations, i.e., the relations of stress and strain, are still assumed to follow the generalized Hooke's law,

$$\sigma_r = \frac{E}{1-\nu^2}(e_r + \nu e_t) \tag{8}$$

and

$$\sigma_t = \frac{E}{1-\nu^2}(e_t + \nu e_r). \tag{9}$$

2.2. Boundary Conditions

Equations (4)–(9) are six governing equations for solving stresses σ_r and σ_t, strains e_r and e_t, and displacements u and w. Equations (4)–(19) can be solved by using the following boundary conditions

$$\frac{\mathrm{d}w}{\mathrm{d}r} = 0 \text{ at } r = 0, \tag{10}$$

$$e_t = 0 \text{ at } r = a \tag{11}$$

and

$$w = 0 \text{ at } r = a. \tag{12}$$

2.3. Power-Series Solutions

Substituting Equations (6) and (7) into Equations (8) and (9) to eliminate e_r and e_t in Equations (8) and (9) yields

$$\sigma_r = \frac{E}{1-\nu^2}\left\{\left[\left(1+\frac{\mathrm{d}u}{\mathrm{d}r}\right)^2+\left(\frac{\mathrm{d}w}{\mathrm{d}r}\right)^2\right]^{1/2}-1+\nu\frac{u}{r}\right\} \tag{13}$$

and

$$\sigma_t = \frac{E}{1-\nu^2}\left\{\frac{u}{r}+\nu\left[\left(1+\frac{\mathrm{d}u}{\mathrm{d}r}\right)^2+\left(\frac{\mathrm{d}w}{\mathrm{d}r}\right)^2\right]^{1/2}-\nu\right\}. \tag{14}$$

Eliminating " $\left[\left(1+\frac{\mathrm{d}u}{\mathrm{d}r}\right)^2+\left(\frac{\mathrm{d}w}{\mathrm{d}r}\right)^2\right]^{1/2}$ " from Equations (13) and (14) and then further eliminating σ_t by Equation (5) yields

$$\frac{u}{r} = \frac{1}{E}(\sigma_t - \nu\sigma_r) = \frac{1}{E}\left[\frac{\mathrm{d}}{\mathrm{d}r}(r\sigma_r) - \nu\sigma_r\right]. \tag{15}$$

After substituting the u in Equation (15) into Equation (14), the usually so-called consistency equation can be written as

$$\begin{array}{c}\left\{\frac{d}{dr}\left[r\frac{d}{dr}(r\sigma_r h)\right]\right\}^2+2Eh\frac{d}{dr}\left[r\frac{d}{dr}(r\sigma_r h)\right]-2v\frac{d}{dr}(r\sigma_r h)\times\frac{d}{dr}\left[r\frac{d}{dr}(r\sigma_r h)\right]\\ +2v\sigma_r h\frac{d}{dr}(r\sigma_r h)-2Eh(\sigma_r h)-(\sigma_r h)^2+E^2h^2\left(\frac{dw}{dr}\right)^2=0\end{array}. \tag{16}$$

Let us proceed to the following nondimensionalization

$$W=\frac{w}{a}, S_r=\frac{\sigma_r}{E}, S_t=\frac{\sigma_t}{E}, x=\frac{r}{a}, H_0=\frac{H}{a}, G=\frac{\rho g a^2}{Eh}, \tag{17}$$

and transform Equations (4), (5), and (16) into

$$4x^2S_r^2\left(-\frac{\mathrm{d}W}{\mathrm{d}x}\right)^2-G^2\left[\left(-\frac{\mathrm{d}W}{\mathrm{d}x}\right)^2+1\right]\left[\int_0^x 2xW(x)\mathrm{d}x+x^2H_0\right]^2=0, \tag{18}$$

$$S_t = S_r + x\frac{\mathrm{d}S_r}{\mathrm{d}x} \tag{19}$$

and

$$\begin{array}{c}\left\{\frac{d}{dx}\left[x\frac{d}{dx}(xS_r)\right]\right\}^2+2\frac{d}{dx}\left[x\frac{d}{dx}(xS_r)\right]-2v\frac{d}{dx}(xS_r)\times\frac{d}{dx}\left[x\frac{d}{dx}(xS_r)\right]\\ +2vS_r\frac{d}{dx}(xS_r)-2S_r-S_r^2+\left(\frac{dW}{dx}\right)^2=0\end{array}. \tag{20}$$

After considering Equations (7) and (15), the boundary conditions, Equations (10)–(12) can be further transformed into

$$\frac{\mathrm{d}W}{\mathrm{d}x} = 0 \text{ at } x=0, \tag{21}$$

$$(1-\nu)S_r + x\frac{\mathrm{d}S_r}{\mathrm{d}x} = 0 \text{ at } x=1 \tag{22}$$

and

$$W = 0 \text{ at } x=1. \tag{23}$$

S_r and W can be solved from Equations (18) and (20). To this end, let us expand S_r and W into the power series in powers of the x, i.e., let

$$S_r = \sum_{i=0}^{\infty} c_i x^i \tag{24}$$

and

$$W = \sum_{i=0}^{\infty} d_i x^i. \tag{25}$$

The recursion formulas for the coefficients c_i and d_i in Equations (24) and (25) can be determined as follows. After substituting Equations (24) and (25) into Equations (18) and (20), the similar terms are combined to obtain the sums of coefficients of the x with the same powers. To ensure that Equations (18) and (20), after being substituted into Equations (24) and (25), still hold regardless of the value taken by the x in the interval [0, 1], all the sums of coefficients of the x with the same powers have to simultaneously be equal to zero. This gives rise to a system containing infinitely more equations with respect to the power-series coefficients c_i and d_i. The recursion formulas for the coefficients c_i and d_i can be determined by successively solving this infinite system of equations, as shown in Appendix A, where the coefficients c_i and d_i are always equal to zero when i is odd, or are expressed as the polynomials of c_0 and d_0 when i is even.

The remaining two coefficients, c_0 and d_0, are usually known as the undetermined constants, and they can be determined by using the boundary conditions at $x = 1$ as follows. From Equation (24), the boundary condition Equation (22) gives

$$(1 - \nu)\sum_{i=0}^{\infty} c_i + \sum_{i=1}^{\infty} i c_i = 0, \tag{26}$$

and from Equation (25), the boundary condition Equation (23) gives

$$\sum_{i=0}^{\infty} d_i = 0. \tag{27}$$

Since all the coefficients c_i and d_i can be expressed as the polynomials of c_0 and d_0 (see the recursion formulas in Appendix A), Equations (26) and (27) contain only the undetermined constants c_0 and d_0. As a result, the undetermined constants c_0 and d_0 can be determined by simultaneously solving Equations (26) and (27), and with the known c_0 and d_0, the expressions of S_r and W can finally be determined. The problem under consideration is thus solved analytically, where the external loads $q(r)$ applied to the circular membrane are defined by the parameter H, i.e., the height of the collected rainwater above the polar plane (r, φ).

2.4. Convergence Analysis of Power-Series Solutions

As can be seen from the Appendix A, the recursion formulas for the coefficients c_i and d_i are so complicated that the convergences of the power-series solutions S_r and W have to be numerically analyzed. To this end, a conductive circular membrane with radius $a = 70$ mm, thickness $h = 0.3$ mm, Young's modulus of elasticity $E = 3.05$ MPa, and Poisson's ratio $\nu = 0.45$, which is subjected to the actions of the collected rainwater with the height $H = 300$ mm and $H = 1000$ mm, respectively, is used as an example to illustrate how to conduct a convergence analysis of the power-series solutions S_r and W.

For the convenience of practical calculation operation, all the infinite power series in Equations (26) and (27) have to be truncated and replaced with their nth partial sums, i.e.,

$$(1 - \nu)\sum_{i=0}^{n} c_i + \sum_{i=1}^{n} i c_i = 0 \tag{28}$$

and

$$\sum_{i=0}^{n} d_i = 0. \tag{29}$$

The undetermined constants c_0 and d_0 are calculated by using Equations (28) and (29), where the value of the parameter n begins first with 2, then $n = 4$, $n = 6$, ..., and does not stop until the calculated numerical values of c_0 and d_0 are sufficiently saturated, as

shown in Table 1, where H = 300 mm. The variations of c_0 and d_0 with n are shown in Figures 3 and 4. It can be seen from Figures 3 and 4 that c_0 and d_0 converge very well as the parameter n progressively increases. Therefore, the coefficients c_i and d_i can be calculated using c_0 = 0.19801 and d_0 = 0.38702301, i.e., the saturated values of b_0 and d_0 when n = 34 in Table 1, and the calculated results of c_i and d_i are listed in Table 2. The variations of c_i and d_i with i are shown in Figures 5 and 6. It can be seen from Figures 5 and 6 that c_i and d_i converge very quickly as i progressively increases. This means that the power-series solutions of stress and deflection converge very well at the right end of the interval $x \in [0, 1]$, i.e., at x = 1. On the other hand, the power-series solutions of stress and deflection converge to c_0 and d_0 at the left end of the interval $x \in [0, 1]$ (i.e., at x = 0, see Equations (24) and (25)); therefore, they converge in the whole interval $x \in [0, 1]$.

Table 1. The numerical values of c_0 and d_0 calculated using different n when a = 70 mm, h = 0.3 mm, E = 3.05 MPa, ν = 0.45, and H = 300 mm.

n	c_0	d_0
2	1.6096321×10^{-1}	3.8879863×10^{-1}
4	1.8256583×10^{-1}	4.0353242×10^{-1}
6	1.8997545×10^{-1}	4.0096550×10^{-1}
8	1.9331984×10^{-1}	3.9755283×10^{-1}
10	1.9507474×10^{-1}	3.9487555×10^{-1}
12	1.9608889×10^{-1}	3.9291886×10^{-1}
14	1.9671601×10^{-1}	3.9135900×10^{-1}
16	1.9712404×10^{-1}	3.9006109×10^{-1}
18	1.9739921×10^{-1}	3.8969211×10^{-1}
20	1.9759256×10^{-1}	3.8911582×10^{-1}
22	1.9773075×10^{-1}	3.8857772×10^{-1}
24	1.9783209×10^{-1}	3.8804093×10^{-1}
26	1.9790780×10^{-1}	3.8747951×10^{-1}
28	1.9796534×10^{-1}	3.8727428×10^{-1}
30	1.9799512×10^{-1}	3.8715202×10^{-1}
32	1.9800913×10^{-1}	3.8703145×10^{-1}
34	1.9801000×10^{-1}	3.8702301×10^{-1}

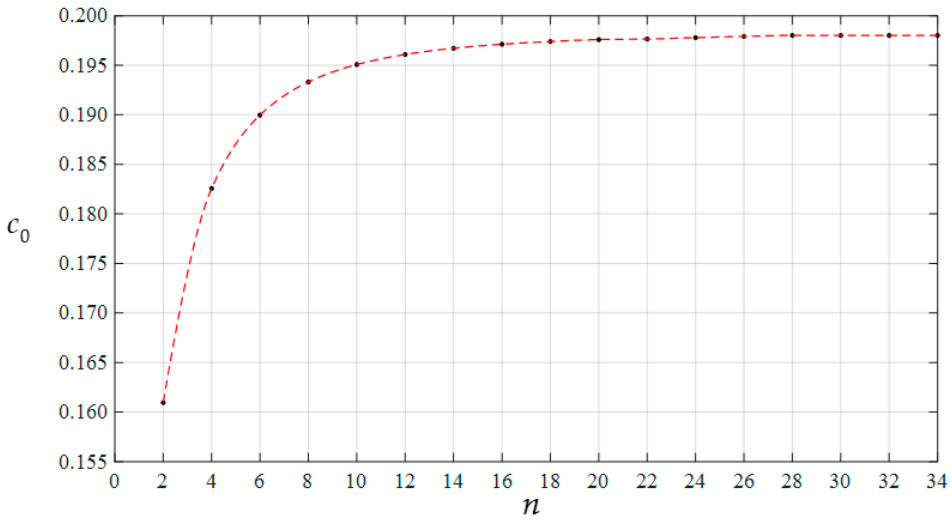

Figure 3. Variation of c_0 with n when a = 70 mm, h = 0.3 mm, E = 3.05 MPa, ν = 0.45, and H = 300 mm.

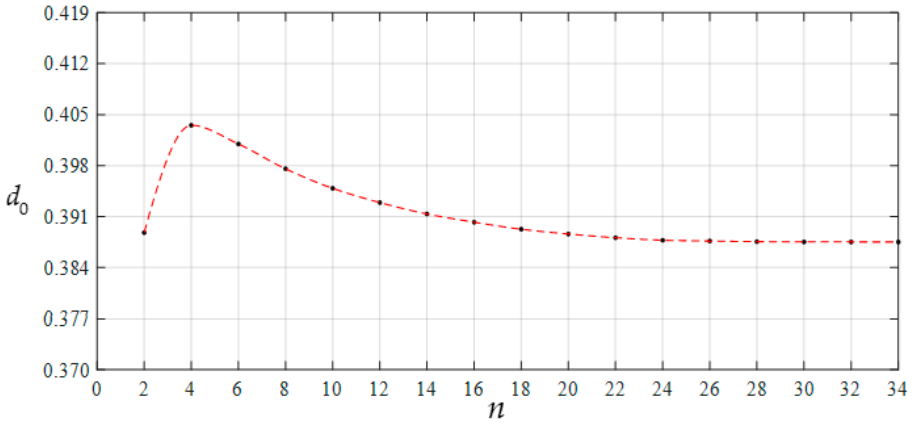

Figure 4. Variation of d_0 with n when a = 70 mm, h = 0.3 mm, E = 3.05 MPa, ν = 0.45, and H = 300 mm.

Table 2. The numerical values of c_i and d_i calculated using c_0 = 0.19801 and d_0 = 0.38702301 when a = 70 mm, h = 0.3 mm, E = 3.05 MPa, ν = 0.45, and H = 300 mm.

i	c_i	d_i
0	1.9801000×10^{-1}	3.8702301×10^{-1}
2	$-2.2503182 \times 10^{-2}$	$-3.1593609 \times 10^{-1}$
4	$-4.7482704 \times 10^{-3}$	$-4.4147582 \times 10^{-2}$
6	$-1.6728142 \times 10^{-3}$	$-1.4480307 \times 10^{-2}$
8	$-7.4018474 \times 10^{-4}$	$-6.0976418 \times 10^{-3}$
10	$-3.7351168 \times 10^{-4}$	$-3.0261953 \times 10^{-3}$
12	$-2.0567441 \times 10^{-4}$	$-1.4010811 \times 10^{-3}$
14	$-1.2065107 \times 10^{-4}$	$-7.9474886 \times 10^{-4}$
16	$-7.4301711 \times 10^{-5}$	$-4.2051265 \times 10^{-4}$
18	$-4.7576760 \times 10^{-5}$	$-2.1235107 \times 10^{-4}$
20	$-3.5862468 \times 10^{-5}$	$-1.9217554 \times 10^{-4}$
22	$-2.1382054 \times 10^{-5}$	$-1.1071414 \times 10^{-4}$
24	$-1.4877621 \times 10^{-5}$	$-7.7178828 \times 10^{-5}$
26	$-1.0567262 \times 10^{-5}$	$-5.0111706 \times 10^{-5}$
28	$-7.6436405 \times 10^{-6}$	$-3.2987094 \times 10^{-5}$
30	$-5.6194073 \times 10^{-6}$	$-2.1986210 \times 10^{-5}$
32	$-4.1919107 \times 10^{-6}$	$-1.4822624 \times 10^{-5}$
34	$-3.1684580 \times 10^{-6}$	$-1.0100267 \times 10^{-5}$

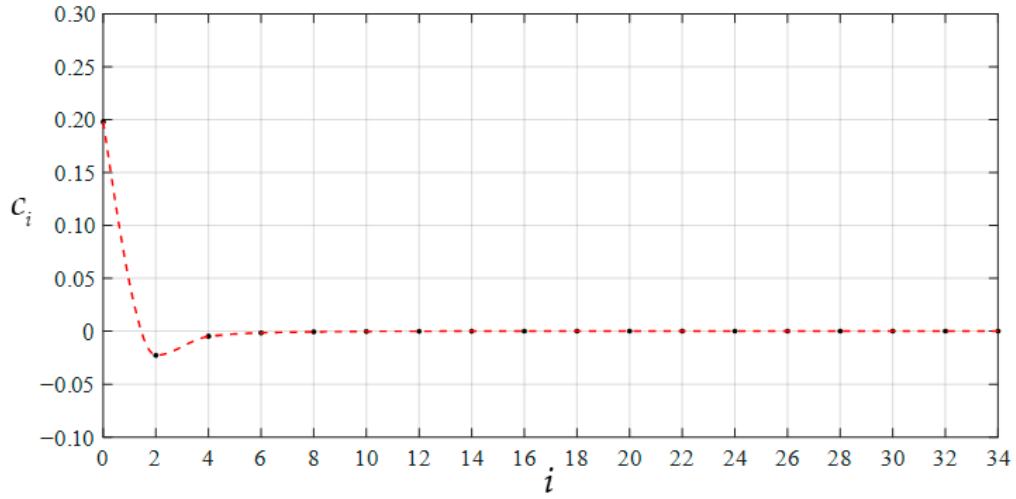

Figure 5. Variation of c_i with i when a = 70 mm, h = 0.3 mm, E = 3.05 MPa, ν = 0.45, and H = 300 mm.

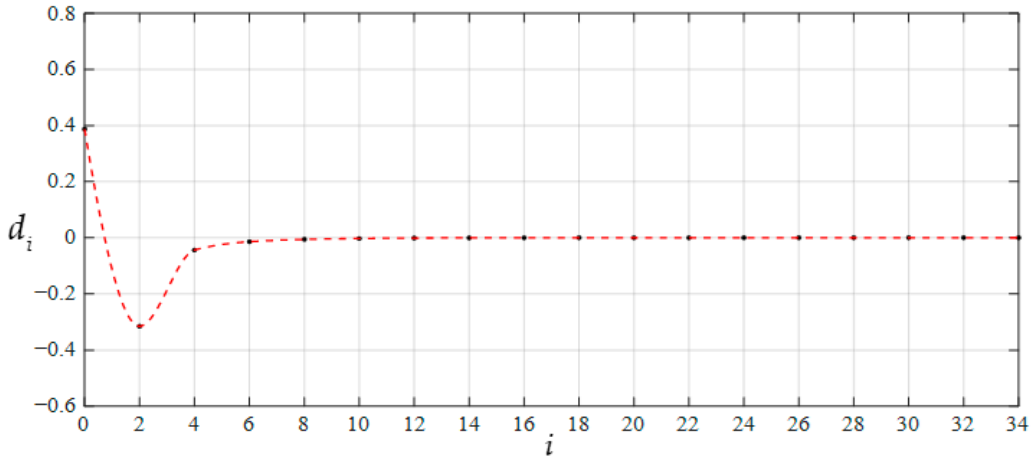

Figure 6. Variation of d_i with i when a = 70 mm, h = 0.3 mm, E = 3.05 MPa, ν = 0.45, and H = 300 mm.

Moreover, the calculated numerical values of c_0 and d_0 for H = 1000 mm are listed in Table 3. The variations of c_0 and d_0 with n are shown in Figures 7 and 8. It can be seen from Figures 7 and 8 that c_0 and d_0 also converge very well for H = 1000 mm. The coefficients c_i and d_i are calculated using c_0 = 0.49259866 and d_0 = 0.55707220, i.e., the saturated values of b_0 and d_0 when n = 40 in Table 3, and the calculated results of c_i and d_i are listed in Table 4. The variations of c_i and d_i with i are shown in Figures 9 and 10. It can be seen from Figures 9 and 10 that c_i and d_i also converge very quickly. Therefore, when H = 1000 mm, the power-series solutions of stress and deflection also converge in the whole interval $x \in [0, 1]$.

Table 3. The numerical values of c_0 and d_0 calculated using different n when a = 70 mm, h = 0.3 mm, E = 3.05 MPa, ν = 0.45, and H = 1000 mm.

n	c_0	d_0
2	3.3839845×10^{-1}	5.8846359×10^{-1}
4	4.0702919×10^{-1}	6.3457560×10^{-1}
6	4.3696963×10^{-1}	6.3275950×10^{-1}
8	4.5326724×10^{-1}	6.2343005×10^{-1}
10	4.6334148×10^{-1}	6.1364387×10^{-1}
12	4.7011936×10^{-1}	6.0483459×10^{-1}
14	4.7496794×10^{-1}	5.9718707×10^{-1}
16	4.7860304×10^{-1}	5.9059016×10^{-1}
18	4.8143206×10^{-1}	5.8407944×10^{-1}
20	4.8380208×10^{-1}	5.7830109×10^{-1}
22	4.8587068×10^{-1}	5.7262599×10^{-1}
24	4.8774255×10^{-1}	5.6754944×10^{-1}
26	4.8932959×10^{-1}	5.6428763×10^{-1}
28	4.9000625×10^{-1}	5.6247383×10^{-1}
30	4.9075866×10^{-1}	5.6025188×10^{-1}
32	4.9149346×10^{-1}	5.5858188×10^{-1}
34	4.9227867×10^{-1}	5.5723711×10^{-1}
36	4.9240450×10^{-1}	5.5719711×10^{-1}
38	4.9253201×10^{-1}	5.5713711×10^{-1}
40	4.9259866×10^{-1}	5.5707220×10^{-1}

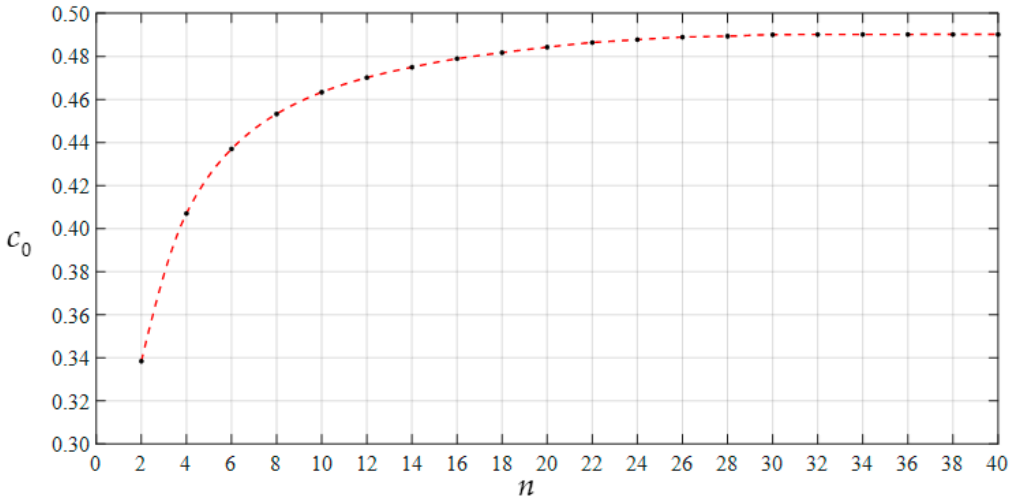

Figure 7. Variation of c_0 with n when a = 70 mm, h = 0.3 mm, E = 3.05 MPa, ν = 0.45, and H = 1000 mm.

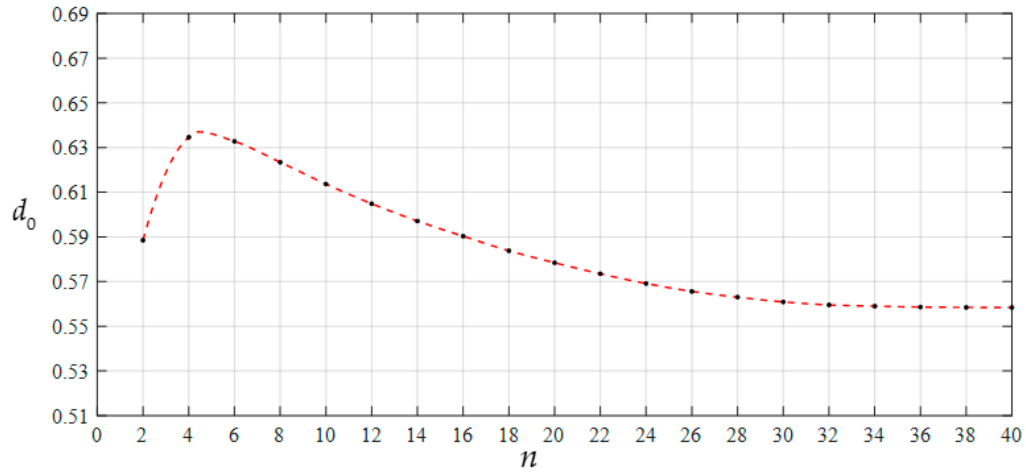

Figure 8. Variation of d_0 with n when a = 70 mm, h = 0.3 mm, E = 3.05 MPa, ν = 0.45, and H = 1000 mm.

Table 4. The numerical values of c_i and d_i calculated using c_0 = 0.49259866 and d_0 = 0.5570722 when a = 70 mm, h = 0.3 mm, E = 3.05 MPa, ν = 0.45, and H = 1000 mm.

i	c_i	d_i
0	4.9259866×10^{-1}	5.5707220×10^{-1}
2	$-3.2010543 \times 10^{-2}$	$-4.0340122 \times 10^{-1}$
4	$-9.0232331 \times 10^{-3}$	$-7.6012684 \times 10^{-2}$
6	$-4.0233576 \times 10^{-3}$	$-3.0795960 \times 10^{-2}$
8	$-2.2202114 \times 10^{-3}$	$-1.6031626 \times 10^{-2}$
10	$-1.3908635 \times 10^{-3}$	$-9.4849784 \times 10^{-3}$
12	$-9.4956383 \times 10^{-4}$	$-6.0706292 \times 10^{-3}$
14	$-6.9066665 \times 10^{-4}$	$-4.0999474 \times 10^{-3}$
16	$-5.2777370 \times 10^{-4}$	$-2.8805707 \times 10^{-3}$
18	$-4.1977975 \times 10^{-4}$	$-2.0867243 \times 10^{-3}$
20	$-3.0524980 \times 10^{-4}$	$-1.3494309 \times 10^{-3}$
22	$-2.5218835 \times 10^{-4}$	$-1.1744272 \times 10^{-3}$
24	$-2.3349516 \times 10^{-4}$	$-8.0307410 \times 10^{-4}$
26	$-2.2477177 \times 10^{-4}$	$-6.1001658 \times 10^{-4}$
28	$-2.0318916 \times 10^{-4}$	$-5.5124579 \times 10^{-4}$

Table 4. *Cont.*

i	c_i	d_i
30	$-1.7687008 \times 10^{-4}$	$-4.4422360 \times 10^{-4}$
32	$-1.3653613 \times 10^{-4}$	$-3.5009484 \times 10^{-4}$
34	$-1.0429799 \times 10^{-4}$	$-3.0502913 \times 10^{-4}$
36	$-6.5852655 \times 10^{-5}$	$-2.3420090 \times 10^{-4}$
38	$-4.3771181 \times 10^{-5}$	$-2.0414329 \times 10^{-4}$
40	$-3.0706861 \times 10^{-5}$	$-1.8232860 \times 10^{-4}$

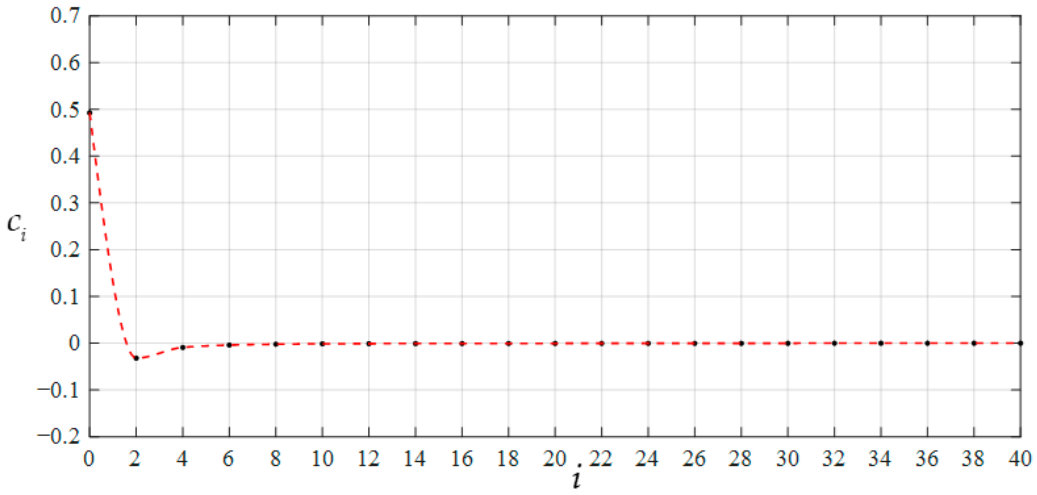

Figure 9. Variation of c_i with i when a = 70 mm, h = 0.3 mm, E = 3.05 MPa, ν = 0.45, and H = 1000 mm.

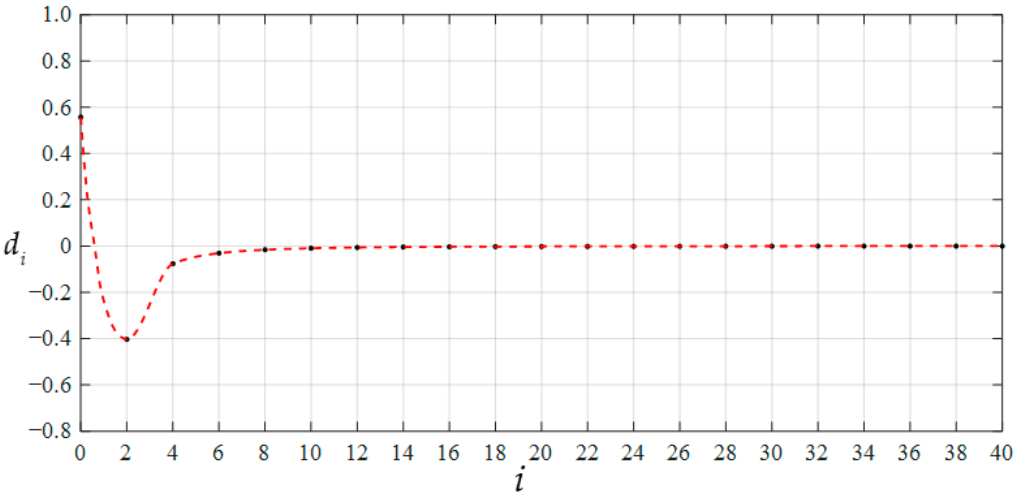

Figure 10. Variation of d_i with i when a = 70 mm, h = 0.3 mm, E = 3.05 MPa, ν = 0.45, and H = 1000 mm.

3. Numerical Calibration of Membrane Deflection-Based Linear Rain Gauges

3.1. Input–Output Analytical Relationships of Membrane Deflection-Based Rain Gauges

Figure 11 shows the states of a membrane deflection-based rain gauge, where the initial state refers to the case without the rainwater, and the operating state refers to the case of the conductive circular membrane (the upper electrode plate) under the rainwater.

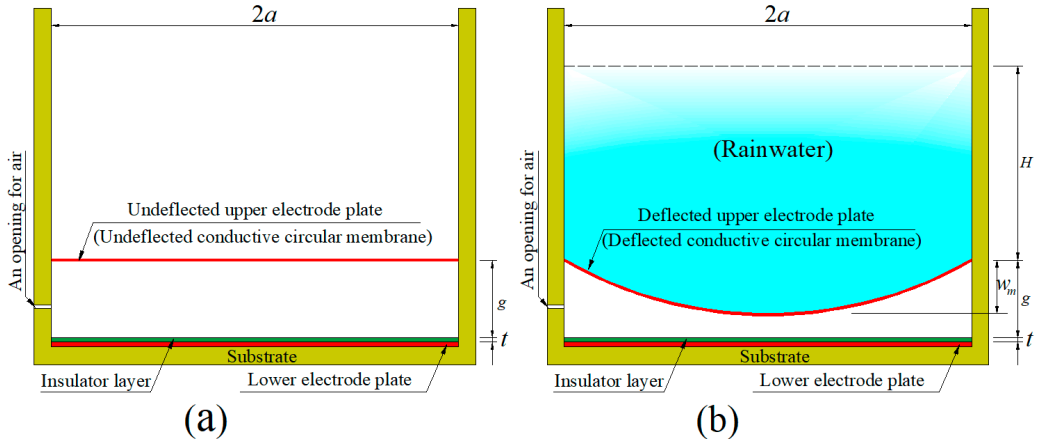

Figure 11. Sketch of a rain gauge: (**a**) initial state and (**b**) operating state.

As shown in Figure 11a, before application of the collected rainwater, the conductive circular membrane (the upper electrode plate) is in its initially flat, undeflected state, maintains an initial parallel gap g with the insulator layer with thickness t, and forms a parallel plate capacitor with the insulator layer. Obviously, the total parallel plate capacitor between the upper and lower electrode plates, whose capacitance is assumed to be denoted as C_0, is comprised of two parallel plate capacitors in series: one is the parallel plate capacitor between the initially undeflected upper electrode plate and the insulator layer, whose capacitance is denoted by C_1, and the other is the one between the insulator layer and the lower electrode plate fixed to the substrate, whose capacitance is denoted by C_2. If the vacuum permittivity is denoted by ε_0, the relative permittivity of air is ε_{r1}, and the relative permittivity of the insulator layer with thickness t is ε_{r2}, then, the capacitance of the parallel plate capacitor between the initially undeflected upper electrode plate and the insulator layer may be written as:

$$C_1 = \frac{\varepsilon_0 \varepsilon_{r1} \pi a^2}{g}, \tag{30}$$

and the capacitance of the parallel plate capacitor between the insulator layer and the lower electrode plate may be written as:

$$C_2 = \frac{\varepsilon_0 \varepsilon_{r2} \pi a^2}{t}. \tag{31}$$

Since the reciprocal of the equivalent capacitance of a series capacitor is equal to the sum of the reciprocal of each series capacitor, the total capacitance of the parallel plate capacitor between the initially undeflected upper electrode plate and the lower electrode plates may be written as:

$$C_0 = \frac{C_1 C_2}{C_1 + C_2} = \frac{\frac{\varepsilon_0 \varepsilon_{r1} \pi a^2}{g} \frac{\varepsilon_0 \varepsilon_{r2} \pi a^2}{t}}{\frac{\varepsilon_0 \varepsilon_{r1} \pi a^2}{g} + \frac{\varepsilon_0 \varepsilon_{r2} \pi a^2}{t}} = \frac{\pi a^2 \varepsilon_0 \varepsilon_{r1} \varepsilon_{r2}}{\varepsilon_{r1} t + \varepsilon_{r2} g}. \tag{32}$$

On the other hand, after application of the collected rainwater, as shown in Figure 11b, the conductive circular membrane (the upper electrode plate) is in a deflected state, whose spatial geometry is governed by the deflection solution: $w(r) = a \sum_{i=0}^{\infty} d_i (\frac{r}{a})^i$, see Equations (17) and (25). Therefore, at this time, the capacitor between the upper electrode plate and the insulator layer is changed from the original parallel plate capacitor with the capacitance C_1 to the current, non-parallel plate capacitor with the capacitance C_1' . The expression of capacitance C_1' can be derived as follows. A micro-area element, which is

formed by the increments of radial coordinate Δr and circumferential coordinate $\Delta\varphi$, is taken, whose area ΔS may be written as:

$$\Delta S = \frac{(r+\Delta r)^2\Delta\varphi}{2} - \frac{r^2\Delta\varphi}{2} = r\Delta r\Delta\varphi + \frac{1}{2}(\Delta r)^2\Delta\varphi. \tag{33}$$

Therefore, ΔS can be reduced to $r\Delta r\Delta\varphi$ after ignoring the higher-order terms in Equation (33). Obviously, this micro-area element still corresponds to a non-parallel plate capacitor. However, since it can be made very small, this non-parallel plate capacitor can be approximately regarded as a parallel plate capacitor with a parallel gap g-$w(r)$, whose capacitance $\Delta C_1'$ may be approximated as:

$$\Delta C_1' = \varepsilon_0\varepsilon_{r1}\frac{r\Delta r\Delta\varphi}{g-w(r)}. \tag{34}$$

By integrating both sides of Equation (34), the capacitance C_1' of the non-parallel plate capacitor between the deflected upper electrode plate and the insulator layer may finally be written as:

$$C_1' = \int_0^a\int_0^{2\pi}\varepsilon_0\varepsilon_{r1}\frac{r}{g-w(r)}\mathrm{d}\varphi\mathrm{d}r = 2\pi\varepsilon_0\varepsilon_{r1}\int_0^a\frac{r}{g-w(r)}\mathrm{d}r. \tag{35}$$

Therefore, the total capacitance C of the non-parallel plate capacitor between the deflected upper electrode plate and the lower electrode plate may finally be written as:

$$C = \frac{C_1'C_2}{C_1'+C_2} = \frac{2\pi a^2\varepsilon_0\varepsilon_{r1}\varepsilon_{r2}\int_0^a\frac{r}{g-w(r)}\mathrm{d}r}{2\varepsilon_{r1}t\int_0^a\frac{r}{g-w(r)}\mathrm{d}r + \varepsilon_{r2}a^2}. \tag{36}$$

Obviously, before application of the collected rainwater, the upper electrode plate (the conductive circular membrane) is in its initially flat, undeflected state, that is, $w(r) \equiv 0$. Therefore, it can be seen by comparing Equation (36) with Equation (32), such that Equation (36) is able to regress to Equation (32) if $w(r)$ in Equation (36) is set equal to 0. This implies that the derivation of Equation (36) is correct.

However, as seen in Section 2, the closed-form solutions of the conductive circular membrane under the action of the liquid loads $q(r)$ are presented in power-series form, the external loads $q(r)$ applied to the conductive circular membrane are defined by the parameter H (the height of the collected rainwater above the polar plane (r, φ)), and all the power-series coefficients of the stress and deflection solutions are dependent on the parameter H (see Appendix A). This means that Equation (36) yields the analytical relationship between the total capacitance C and the rainwater height H, rather than the desired analytical relationship between the total capacitance C and the rainwater volume V, which is essential to the numerical calibration of the rain gauge to be designed. Therefore, the volume V of the rainwater collected in the rainwater-collecting tank can only be determined after the deflection solution $w(r)$ is determined with the parameter H. To this end, a micro-volume element, which is formed by the approximate height, $H + w(r)$, and the increments of the radial coordinate Δr and circumferential coordinate $\Delta\varphi$, is taken, whose volume ΔV may be approximated as:

$$\Delta V = [H+w(r)][\frac{(r+\Delta r)^2\Delta\varphi}{2} - \frac{r^2\Delta\varphi}{2}] = [H+w(r)][r\Delta\varphi\Delta r + \frac{1}{2}\Delta\varphi(\Delta r)^2]. \tag{37}$$

Therefore, ΔV can be reduced to $[H + w(r)]r\Delta r\Delta\varphi$ after ignoring the higher-order terms in Equation (37). By integrating both sides of Equation (37), the volume V of the rainwater collected in the rainwater-collecting tank may finally be written as:

$$V = \int_0^a\int_0^{2\pi}[H+w(r)]r\mathrm{d}\varphi\mathrm{d}r = \pi r^2H + 2\pi\int_0^a w(r)r\mathrm{d}r. \tag{38}$$

As stated in the Introduction Section, the basic principle of this rain gauge is to determine the rainwater volume V by measuring the total capacitance C, which implies that the measured capacitance C is used as input and the volume V to be determined is used as output. This can be achieved by substituting the $w(r)$ in Equations (36)–(38). Obviously, however, doing so works only in theory, not in practice, due to the strong nonlinearity therein; that is, the relationship between the input capacitance C and output volume V has strong nonlinearity.

3.2. Numerical Calculation of Nonlinear Input–Output Relationships

The proposed membrane deflection-based rain gauges generally need to first be numerically calibrated before the experimental calibration. In other words, in order to reduce unnecessary economic losses, material purchase, fabrication, and experimental calibration can only be considered on the basis of sufficient numerical design and calibration. During the design stage of a membrane deflection-based rain gauge, the stress solution provided in Section 2 is used to calculate the maximum stress, σ_{m}, of the conductive circular membrane under the action of the collected rainwater, to ensure that the membrane will not yield during normal operation. The relationship between input capacitance C and output volume V has to be graphically presented based on numerical calculations, due to its strong nonlinearity (see Equations (36) and (38)). In the following, an example is provided to illustrate how to carry out the numerical calculation and calibration of the relationship between input capacitance C and output volume V.

The total capacitance C of the non-parallel plate capacitor between the deflected upper electrode plate and the lower electrode plate (see Figure 11) can be calculated by Equation (36), while the volume V of the rainwater collected in the rainwater-collecting tank can be calculated by Equation (38). For comparison under the same conditions, the $w(r)$ in Equations (36) and (38) is determined by using the deflection solutions provided in this paper and in [13], respectively. Finally, using the calculated results of input capacitance C and output volume V, the relationships between the input capacitance C and output volume V can be graphically presented. Suppose that in Figure 11, the conductive circular membrane with radius a = 70 mm, thickness h = 0.3 mm, and Poisson's ratio ν = 0.45 is subjected to the action of the collected rainwater with the height H that progressively increases from 0 mm to 1160 mm, and its Young's modulus of elasticity, E, is 7.84 MPa, 3.05 MPa, and 1.55 MPa, respectively. The initial parallel gap between the initially undeflected upper electrode plate (the undeflected conductive circular membrane) and the insulator layer, g, is 45 mm, the thickness of the insulator layer, t, is 0.1 mm, the vacuum permittivity, ε_0, is $8.854187817 \times 10^{-12}$ F/m, the relative permittivity of air, ε_{r1}, is 1.000585, and the relative permittivity of the insulator layer (polystyrene), ε_{r2}, is 2.5.

The numerical results calculated by using the deflection solutions presented in Section 2, including the volume V and height H of the applied rainwater, the undetermined constants c_0 and d_0, the maximum stress σ_{m} and maximum deflection w_{m} of the conductive circular membrane, and the total capacitance C, are listed in Table 5 for E = 7.84 MPa, in Table 6 for E = 3.05 MPa, and in Table 7 for E = 1.55 MPa, respectively. The numerical results calculated by using the deflection solutions presented in [13] are listed in Table 8 for E = 7.84 MPa, in Table 9 for E = 3.05 MPa, and in Table 10 for E = 1.55 MPa, respectively. The graphical relationships between the input capacitance C and output volume V are shown in Figure 12 for E = 7.84 MPa, in Figure 13 for E = 3.05 MPa, and in Figure 14 for E = 1.55 MPa, respectively, where "Solution 1" refers to the results calculated by using the deflection solution provided in Section 2, and "Solution 2" refers to the results calculated by using the deflection solution presented in [13].

Table 5. The calculation results obtained by using the deflection solution presented in Section 2, when a = 70 mm, h = 0.3 mm, E = 7.84 MPa, ν = 0.45, t = 0.1 mm, and g = 45 mm.

V/mm^3	H/mm	c_0	d_0	σ_m/MPa	w_m/mm	C/pF
0	0	0	0	0	0	3.031
124,575	5	0.00912651	0.08928599	0.072	6.250	3.260
375,589	20	0.01804884	0.12363215	0.142	8.654	3.372
858,653	50	0.03086522	0.16028735	0.242	11.220	3.501
1,334,678	80	0.04136554	0.18472239	0.324	12.931	3.595
1,650,327	100	0.04768439	0.19800761	0.374	13.861	3.649
2,435,732	150	0.06208688	0.22478540	0.487	15.735	3.766
3,218,327	200	0.07514752	0.24648209	0.589	17.254	3.869
4,778,253	300	0.09889744	0.28076362	0.775	19.653	4.049
6,333,912	400	0.12044591	0.30814841	0.944	21.570	4.210
7,888,224	500	0.14112447	0.33158565	1.106	23.211	4.369
9,439,805	600	0.16035428	0.35188757	1.257	24.632	4.515
10,991,294	700	0.17927879	0.37051281	1.406	25.936	4.668
12,542,859	800	0.19780640	0.38824460	1.551	27.177	4.833
14,090,957	900	0.21564079	0.40241204	1.691	28.169	4.967
15,639,301	1000	0.23265806	0.41685058	1.824	29.180	5.117
17,184,907	1100	0.25131599	0.42593509	1.970	29.815	5.221
18,736,165	1200	0.26785971	0.44219936	2.100	30.954	5.462
20,281,633	1300	0.28472526	0.45204828	2.232	31.644	5.670
21,832,194	1400	0.30154191	0.46626571	2.364	32.638	5.848
23,377,102	1500	0.31713399	0.47601986	2.486	33.321	5.058
24,920,726	1600	0.33252186	0.48436690	2.607	33.906	6.251
26,267,341	1700	0.34772280	0.49535388	2.726	34.675	6.451
27,516,958	1800	0.36575166	0.50602041	2.867	35.421	6.637
28,760,027	1900	0.38062130	0.51340029	2.984	35.938	6.860
30,006,149	2000	0.39534296	0.52352253	3.099	36.647	7.082
31,248,954	2100	0.40992652	0.53041230	3.213	37.129	7.347
32,197,815	2200	0.42738078	0.54009150	3.351	37.806	7.582
33,140,390	2300	0.44171346	0.54657935	3.463	38.261	7.840
34,450,957	2400	0.45593168	0.55589281	3.575	38.912	8.214
35,634,503	2500	0.47304169	0.56504691	3.709	39.553	8.586
36,780,016	2600	0.48704925	0.57405502	3.818	40.184	9.068
37,723,326	2700	0.50095953	0.58092913	3.928	40.665	9.546
38,467,637	2800	0.51477727	0.58867998	4.036	41.208	10.288
39,207,668	2900	0.53050684	0.60001726	4.159	42.001	11.555

Table 6. The calculation results obtained by using the deflection solution presented in Section 2, when a = 70 mm, h = 0.3 mm, E = 3.05 MPa, ν = 0.45, t = 0.1 mm, and g = 45 mm.

V/mm^3	H/mm	c_0	d_0	σ_m/MPa	w_m/mm	C/pF
0	0	0	0	0	0	3.031
146,691	5	0.01970885	0.13184277	0.060	9.229	3.385
404,127	20	0.03649575	0.17618466	0.111	12.333	3.549
895,034	50	0.06113101	0.22518344	0.186	15.763	3.758
1,376,699	80	0.08160197	0.25830933	0.249	18.082	3.918
1,695,396	100	0.09405417	0.27623054	0.287	19.336	4.014
2,487,441	150	0.12268822	0.31281998	0.374	21.897	4.232
3,275,452	200	0.14901856	0.34230622	0.455	23.961	4.435
4,842,819	300	0.19812768	0.38702300	0.604	27.091	4.802
6,409,229	400	0.24266300	0.42806925	0.740	29.965	5.232
7,969,683	500	0.28553745	0.46027746	0.871	32.219	5.653
9,527,928	600	0.32846954	0.48689881	1.002	34.083	6.094
11,080,313	700	0.36913154	0.50797866	1.126	35.556	6.496

Table 6. *Cont*.

V/mm^3	H/mm	c_0	d_0	σ_m/MPa	w_m/mm	C/pF
12,632,618	800	0.40776782	0.52917831	1.244	37.042	6.989
14,184,999	900	0.45054965	0.54504372	1.374	38.153	7.479
15,733,468	1000	0.49259866	0.55707220	1.502	38.995	8.067
17,293,779	1100	0.52902425	0.58434882	1.614	40.904	9.136
18,219,213	1159	0.55081967	0.59296547	1.680	41.508	9.784

Table 7. The calculation results obtained by using the deflection solution presented in Section 2, when a = 70 mm, h = 0.3 mm, E = 1.55 MPa, ν = 0.45, t = 0.1 mm, and g = 45 mm.

V/mm^3	H/mm	c_0	d_0	σ_m/MPa	w_m/mm	C/pF
0	0	0	0	0	0	3.031
169,813	5	0.03504216	0.17636915	0.054	12.346	3.530
433,003	20	0.06160905	0.22908031	0.095	16.036	3.758
931,308	50	0.10161546	0.28875958	0.157	20.213	4.069
1,418,300	80	0.13536348	0.32949594	0.209	23.065	4.327
1,740,528	100	0.15660160	0.35132099	0.243	24.592	4.491
2,539,208	150	0.20501025	0.39658974	0.318	27.761	4.882
3,332,226	200	0.24990568	0.43276906	0.387	30.294	5.272
4,911,306	300	0.33517697	0.49068028	0.519	34.348	6.145
6,485,216	400	0.41408249	0.54065885	0.642	37.846	7.336
8,057,472	500	0.49541046	0.58106523	0.768	40.674	9.070
8,843,439	550	0.53204470	0.60338329	0.824	42.237	10.704
9,623,917	600	0.56810397	0.62001403	0.880	43.401	12.794

Table 8. The calculation results obtained by using the deflection solution presented in [13], when a = 70 mm, h = 0.3 mm, E = 7.84 MPa, ν = 0.45, t = 0.1 mm, and g = 45 mm.

V/mm^3	H/mm	c_0	d_0	σ_m/MPa	w_m/mm	C/pF
0	0	0	0	0	0	3.031
124,588	5	0.00913051	0.08929323	0.072	6.251	3.261
375,633	20	0.01806282	0.12365775	0.142	8.656	3.375
858,691	50	0.03089858	0.16029982	0.242	11.221	3.504
1,334,723	80	0.04141489	0.18475348	0.325	12.933	3.599
1,650,384	100	0.04775642	0.19802746	0.374	13.862	3.657
2,435,884	150	0.06217947	0.22494449	0.487	15.741	3.777
3,218,461	200	0.07526571	0.24665732	0.590	17.260	3.881
4,778,663	300	0.09906146	0.28128970	0.777	19.690	4.073
6,335,174	400	0.12084574	0.30925282	0.944	21.648	4.245
7,889,134	500	0.14131148	0.33286392	1.108	23.300	4.409
9,441,679	600	0.16090029	0.35370677	1.261	24.759	4.575
10,992,711	700	0.17955734	0.37244376	1.408	26.071	4.732
12,543,452	800	0.19807130	0.38955350	1.553	27.269	4.905
14,092,787	900	0.21580643	0.40516165	1.692	28.361	5.091
15,641,994	1000	0.23326902	0.42000069	1.829	29.400	5.349
17,191,522	1100	0.25243719	0.43374474	1.971	30.362	5.649
18,739,873	1200	0.27177709	0.44517926	2.131	31.162	5.958
20,290,603	1300	0.29002133	0.47212330	2.274	33.049	6.315
21,850,279	1400	0.30683175	0.49023351	2.406	34.316	6.770
23,810,192	1500	0.31957734	0.51393343	2.505	35.975	7.440
24,921,876	1600	0.33516431	0.53469018	2.628	37.428	8.040
26,273,301	1700	0.35079983	0.55535388	2.750	38.875	8.850
27,526,771	1800	0.36873324	0.58255698	2.891	40.779	9.950
28,771,321	1900	0.38242337	0.60046679	2.998	42.033	11.221
30,029,618	2000	0.39749640	0.62254338	3.116	43.578	12.750

Table 9. The calculation results obtained by using the deflection solution presented in [13], when a = 70 mm, h = 0.3 mm, E = 3.05 MPa, ν = 0.45, t = 0.1 mm, and g = 45 mm.

V/mm^3	H/mm	c_0	d_0	σ_m/MPa	w_m/mm	C/pF
0	0	0	0	0	0	3.031
146,724	5	0.06016640	0.13186295	0.060	9.230	3.386
404,212	20	0.03655238	0.17621740	0.111	12.335	3.551
895,253	50	0.06128064	0.22528736	0.187	15.770	3.759
1,376,928	80	0.08183265	0.25841407	0.250	18.092	3.920
1,695,731	100	0.09432359	0.27647647	0.288	19.353	4.017
2,488,099	150	0.12303213	0.31351195	0.375	21.946	4.238
3,276,555	200	0.14965178	0.34321310	0.456	24.025	4.446
4,846,461	300	0.19821688	0.39148280	0.605	27.404	4.850
6,411,526	400	0.24471626	0.42924903	0.746	30.047	5.261
7,978,001	500	0.29208802	0.46270729	0.891	32.389	5.755
9,540,106	600	0.33782439	0.49102081	1.030	34.371	6.272
11,101,273	700	0.38000127	0.51981346	1.159	36.387	6.926
12,661,746	800	0.42426305	0.54443643	1.294	38.111	7.690
14,221,573	900	0.46737880	0.56833220	1.426	39.783	8.692
15,776,926	1000	0.50487106	0.59139964	1.540	41.398	10.034
17,328,075	1100	0.54153188	0.61012303	1.652	42.709	11.750
18,253,522	1159	0.56126944	0.62057931	1.712	43.441	13.246

Table 10. The calculation results obtained by using the deflection solution presented in [13], when a = 70 mm, h = 0.3 mm, E = 1.55 MPa, ν = 0.45, t = 0.1 mm, and g = 45 mm.

V/mm^3	H/mm	c_0	d_0	σ_m/MPa	w_m/mm	C/pF
0	0	0	0	0	0	3.031
169,902	5	0.03509797	0.17643908	0.054	12.351	3.530
433,137	20	0.06176587	0.22910474	0.096	16.037	3.759
931,759	50	0.10190303	0.28922995	0.158	20.246	4.074
1,419,348	80	0.13587112	0.33052673	0.211	23.137	4.338
1,741,524	100	0.15675307	0.35309502	0.243	24.717	4.504
2,541,171	150	0.20535898	0.39945876	0.318	27.962	4.953
3,335,829	200	0.25076296	0.43702251	0.389	30.592	5.503
4,917,064	300	0.33611589	0.49773713	0.521	34.846	6.827
6,491,273	400	0.41649287	0.54717865	0.646	38.303	8.776
8,061,359	500	0.49382544	0.58981307	0.765	41.287	11.898
8,845,243	550	0.53214314	0.60880232	0.825	42.616	14.857
9,629,215	600	0.56999709	0.62751931	0.883	43.926	18.896

It can be seen from Figures 12–14 that the C-V relationships are indeed nonlinear, and that the difference between the C-V relationship calculated by using the deflection solution provided in this paper and that calculated by using the deflection solution in [13], i.e., the difference between "Solution 1" and "Solution 2" in Figures 12–14, is very clear, and it increases with the increase of the Young's modulus of elasticity E. This difference is caused by the use of the improved differential-integral governing equations (see Section 2). In addition, from Figures 12–14, it can be observed that the ranges of the nearly-linear segments (which seem to follow a linear variation trend) in the nonlinear C-V relationships calculated by using the deflection solution in this paper are wider than the ranges of the nearly-linear segments (which seem to follow a linear variation trend) in the nonlinear C-V relationships calculated by using the deflection solution presented in [13] (see "Solution 1" and "Solution 2" in Figures 12–14). For instance, the ranges of the nearly-linear segments of E = 3.05 MPa are about C = 3.5 pF–8 pF and V = 15,733,468 mm^3 in "Solution 1", and C = 3.5 pF–6 pF and V = 9,540,106 mm^3 in "Solution 2", respectively (see Figure 13). The differences of 2 pF and 6,193,362 mm^3 are very valuable for designing linear rain gauges, especially the 2 pF input capacitance, C. This is caused by the use of the improved differential-integral governing equations in Section 2.

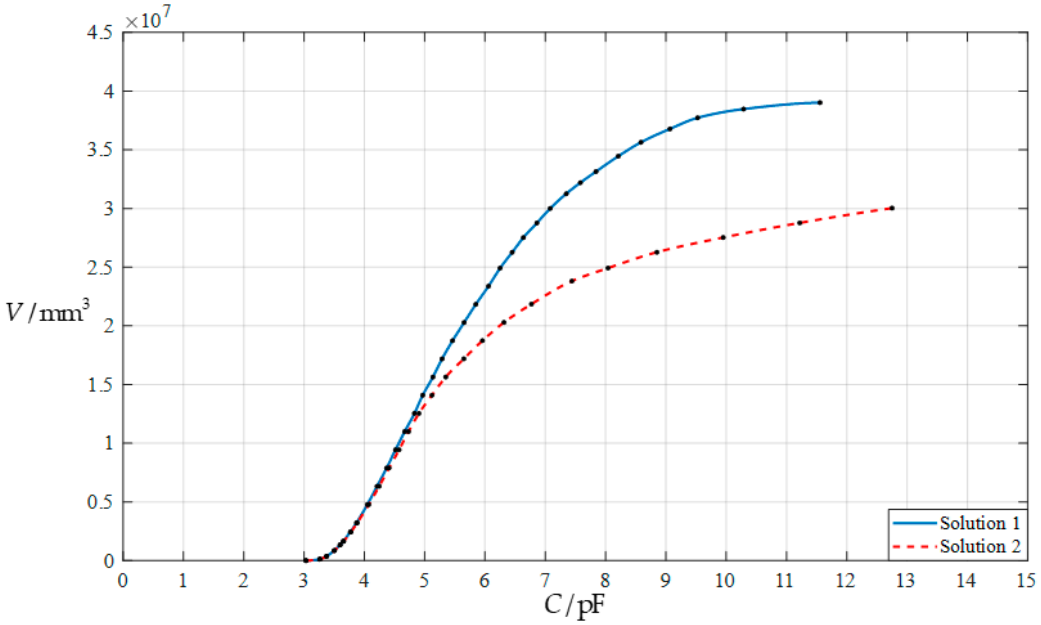

Figure 12. The relationships between the input capacitance C and output volume V when a = 70 mm, h = 0.3 mm, E = 7.84 MPa, ν = 0.45, t = 0.1 mm, and g = 45 mm, where "Solution 1" refers to the results calculated by using the deflection solution presented in Section 2, and "Solution 2" refers to the results calculated by using the deflection solution provided in [13].

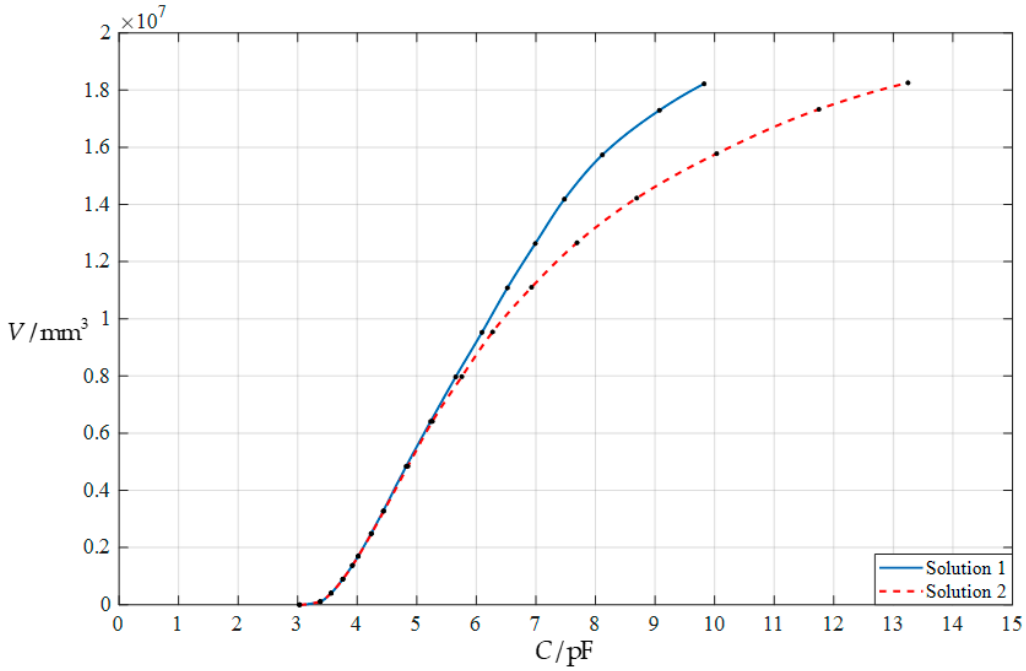

Figure 13. The relationships between the input capacitance C and output volume V when a = 70 mm, h = 0.3 mm, E = 3.05 MPa, ν = 0.45, t = 0.1 mm, and g = 45 mm, where "Solution 1" refers to the results calculated by using the deflection solution presented in Section 2, and "Solution 2" refers to the results calculated by using the deflection solution provided in [13].

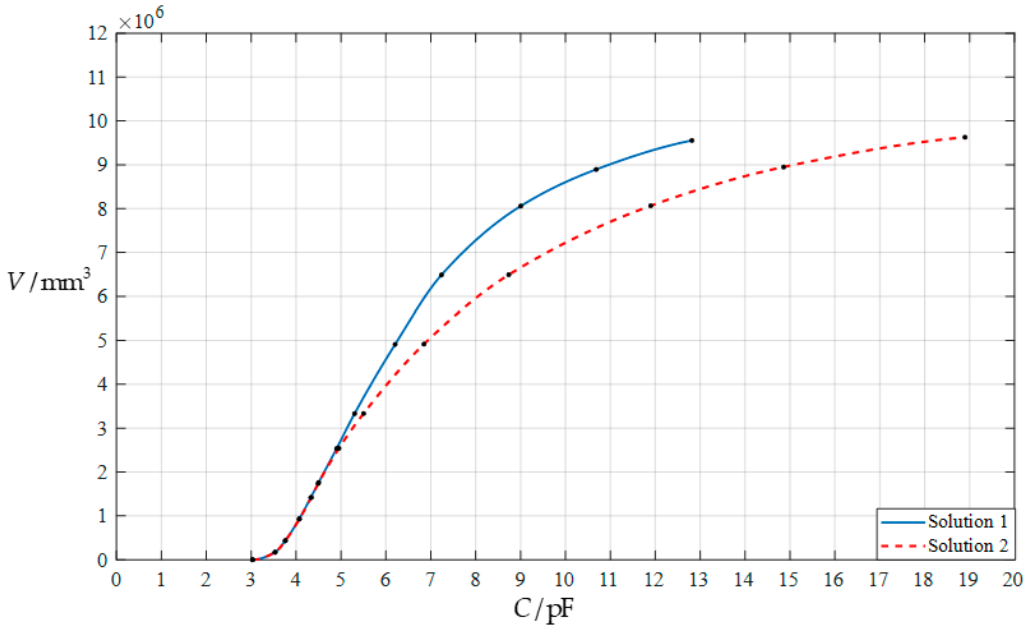

Figure 14. The relationships between the input capacitance C and output volume V when a = 70 mm, h = 0.3 mm, E = 1.55 MPa, ν = 0.45, t = 0.1 mm, and g = 45 mm, where "Solution 1" refers to the results calculated by using the deflection solution presented in Section 2, and "Solution 2" refers to the results calculated by using the deflection solution provided in [13].

3.3. An Example of Numerical Calibration for Linear Rain Gauges

The reason why in [13], only nonlinear rain gauges are discussed, and linear rain gauges are not considered, is that the range of the nearly-linear segment obtained is too narrow for linear fitting. We will not discuss nonlinear fitting here, but only provide an example to illustrate how to conduct the linear fitting for numerically calibrating a linear rain gauge. The data for the output volume V and input capacitance C in Table 6, i.e., 146,691 mm^3–15,733,468 mm^3 for the output volume V and 3.385 pF–8.067 pF for the input capacitance C, are used to numerically calibrate a linear rain gauge, and the obtained linear relationship between the output volume V and input capacitance C is, via least-squares straight-line-fitting,

$$V = 3524947C - 12176469. \tag{39}$$

The fitting effect is shown in Figure 15. Therefore, such a linear rain gauge should be calibrated to about 3525 mm^3 per 1 pF input capacitance C, when designing its analog circuit. Obviously, for any two capacitance measurements, the difference in measured capacitances, ΔC, corresponds to the difference in the rainwater volumes to be measured, ΔV, while the volume difference, ΔV, divided by the time difference between the two capacitance measurements, Δt, is the rainfall volume per unit time. However, it is usually customary to express rainfall by the height of the rainfall per unit area per unit time. For example, if the upward opening area A of the rainwater collector funnel (see Figure 1) is equal to one square meter, and if the height of rainfall is expressed in centimeters, then the rainfall R_f, measured by this linear rain gauge, can be simply calibrated as:

$$R_f = (0.352\Delta C - 1.218)/\Delta t, \tag{40}$$

where R_f is measured in units per centimeter per square meter per unit time, and Δt can be measured in units per second, per minute, per hour, per day, per month, or even per year.

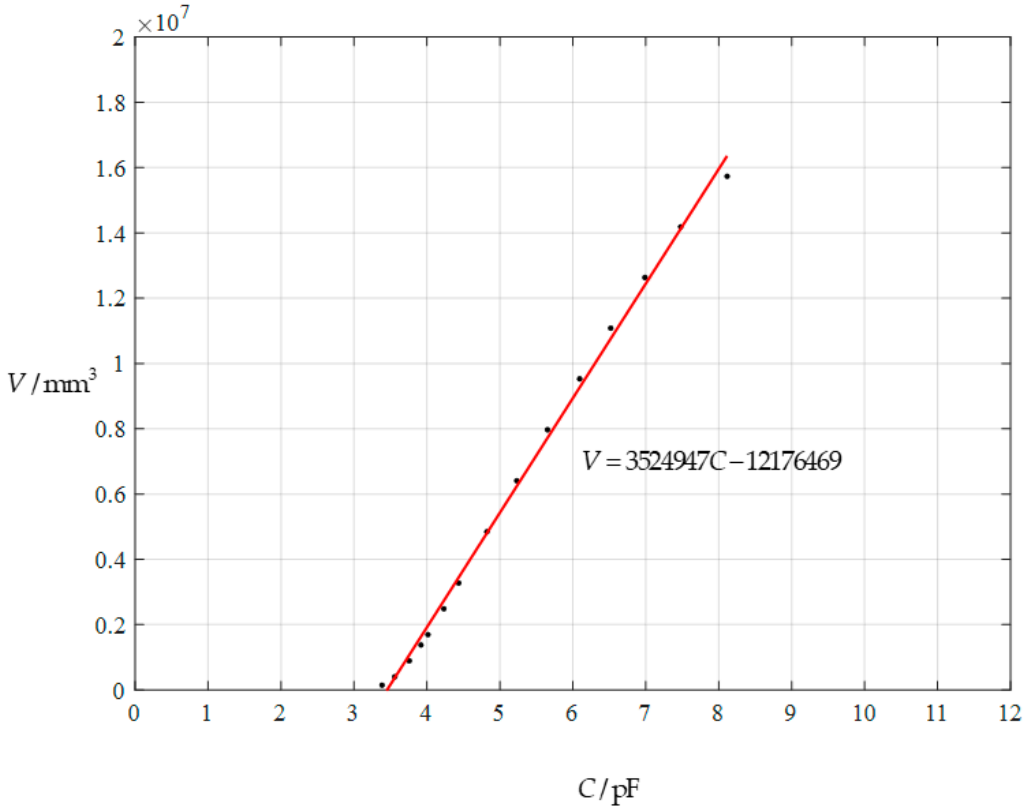

Figure 15. The least-squares straight-line-fitting for the nearly-linear segment of "Solution 1" in Figure 13.

4. Results and Discussion

The membrane elastic deflection-based rain gauges proposed here have the following advantages, in comparison to the traditional tipping-bucket rain gauges (TBRGs) [14–18]. First, unlike tipping-bucket rain gauges, these new types of rain gauges do not need to conduct the calibration for volumetric metering of rainwater, thus avoiding the measurement errors of precipitation caused by this. Second, these new types of rain gauges can achieve continuous rainfall measurements, because the magnitude of the time interval Δt between two measurements of the input capacitance C can be arbitrary, while the time taken to fill a TBRG bucket with rainwater under a given rainfall intensity is basically constant (i.e., the time between two rainfall measurements is basically constant for TBRGs, so the continuous rainfall measurements cannot be achieved.) Therefore, these new types of rain gauges can be used in cases where continuous rainfall measurements are required but cannot be satisfied by TBRGs.

It can be seen from Section 3.2 that the closed-form solution presented in Section 2 is more suitable for designing linear rain gauges, in comparison to the closed-form solution in [13]. It can be seen by comparing Section 2 in this paper with Section 2 in [13] that the out-of-plane and in-plane equilibrium equations, physical equations, and circumferential geometric equation used in this paper are the same as those used in [13], and only the radial geometric equation used in this paper is different from that used in [13]. Therefore, the difference between the power-series solutions presented in this paper and those in [13] is entirely caused by the different radial geometric equations used. The difference between the radial geometric equation used in this paper and that used in [13] can be seen in Section 4.1 below.

The reason for the emphasis on linear rain gauges is that the circuit design of linear sensors is much easier than that of nonlinear sensors. Linear sensors can use analog circuit technology, while nonlinear sensors often can only use digital circuits. Therefore, under the same conditions, the use of a linear sensor has more advantages than the use of a nonlinear sensor, such as simple, easy to implement, low cost, good stability, and strong adaptability

to the use environment. However, if a linear rain gauge is to be designed and calibrated, then the ranges of the input capacitance C as well as the output volume V are usually difficult to fully meet the actual use requirements. At this time, it is often necessary to consider making some compromises, otherwise, the rain gauge design cannot proceed, as is often the case with the solutions of many engineering problems [35–40]. Therefore, in this sense, linear rain gauge designs are usually much more difficult, in comparison to nonlinear rain gauge designs.

In addition, it is obvious that the power-series solutions must be shown to converge before they can be used in practical computational applications. In other words, a particular solution in the form of a power series must be analyzed for convergence before it can be used, otherwise it cannot be used. However, the problem dealt with here, the liquid–structure interaction of the circular membrane under liquid weight loading (see Figure 1 and Equation (1)), presents a strong nonlinearity. This leads to the phenomenon that the characteristic parameters of the problem, the undetermined constants c_0 and d_0, strictly depend on the external action $q(r)$ applied to the circular membrane, which is defined by the height H of the collected rainwater above the polar plane (r, φ) (see Figure 11). Therefore, every value of H corresponds to a statics problem, a pair of saturated values of c_0 and d_0, which are calculated by progressively increasing the parameter n, and a pair of particular solutions of stress and deflection, which need to be shown to converge, as detailed in Section 2.4. As a result, a lot of numerical calculations and convergence analyses are needed to obtain a usable pair of particular solutions of stress and deflection. Therefore, from this point of view, it is very important to carry out research on various computational approaches [41,42].

As can be seen in Section 3.2, the closed-form solution presented in this paper has a positive effect on changing the range of the nearly-linear segment. In addition, changing some design parameters, such as Young's modulus of elasticity E and Poisson's ratio ν, can also influence the range of the nearly-linear segment in the nonlinear relationships between the input capacitance C and the output volume V, as can be seen in Sections 4.2 and 4.3 below.

4.1. Difference between Geometric Equations Used Here and Those Used in [13]

The geometric equations, i.e., the analytical relationships between displacements and strains, are derived by taking radial and circumferential micro-line elements on the circular membrane before and after deformation. Imagine that the conductive circular membrane undergoes an axisymmetric deformation with large deflection under the collected rainwater (see Figure 11); therefore, a radial micro-straight-line element $\overline{A'B'}$ on the initially flat circular membrane before deformation becomes a radial micro-curve element $\overset{\frown}{AB}$ on the circular membrane after deformation, as shown in Figure 16a, while a circumferential micro-curve element $\overset{\frown}{A'D'}$ on the initially flat circular membrane before deformation becomes a circumferential micro-curve element $\overset{\frown}{AD}$ on the circular membrane after deformation, as shown in Figure 16b. The initial length of $\overline{A'B'}$ is Δr, see Figure 16a, and the increment of the polar angle coordinate φ is $\Delta\varphi$; that is, the angle of counterclockwise rotation from the point A' to the point D', see Figure 16b. The coordinate of the point A' is $(r, \varphi, 0)$, and its radial and transverse displacements are denoted by u and w, respectively; that is, the coordinate of the point A is $(r + u, \varphi, w)$. The coordinate of the point B' is $(r + \Delta r, \varphi, 0)$, and its radial and transverse displacements may be expressed as $u(r + \Delta r)$ and $w(r + \Delta r)$, respectively. Therefore, after expanding $u(r + \Delta r)$ and $w(r + \Delta r)$ into the Taylor series and ignoring the higher-order terms therein, that is, letting

$$u(r+\Delta r) = u(r) + \frac{\mathrm{d}u(r)}{\mathrm{d}r}\Delta r + \frac{1}{2!}\frac{\mathrm{d}^2u(r)}{\mathrm{d}r^2}(\Delta r)^2 + \ldots \cong u(r) + \frac{\mathrm{d}u(r)}{\mathrm{d}r}\Delta r \tag{41}$$

and

$$w(r+\Delta r) = w(r) + \frac{\mathrm{d}w(r)}{\mathrm{d}r}\Delta r + \frac{1}{2!}\frac{\mathrm{d}^2 w(r)}{\mathrm{d}r^2}(\Delta r)^2 + \ldots \cong w(r) + \frac{\mathrm{d}w(r)}{\mathrm{d}r}\Delta r, \tag{42}$$

the geometric dimensions marked on Figure 16a can be obtained.

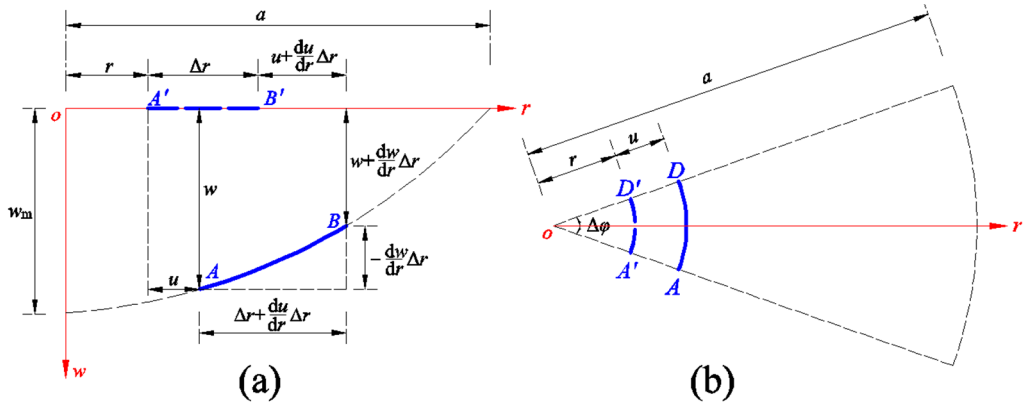

Figure 16. Geometrical relationships of micro-line elements before and after deformation: (**a**) The geometrical relationship between a radial micro-straight-line element $\overline{A'B'}$ before deformation and a radial micro-curve element $\overset{\frown}{AB}$ after deformation. (**b**) The geometrical relationship between a circumferential micro-curve element $\overset{\frown}{A'D'}$ before deformation and a circumferential micro-curve element $\overset{\frown}{AD}$ after deformation.

According to the definition of line strain, the radial line strain when the radial micro-straight-line element $\overline{A'B'}$ becomes the radial micro-curve element $\overset{\frown}{AB}$ may be written as (see Figure 16a)

$$e_r = \frac{L_{\overset{\frown}{AB}} - L_{\overline{A'B'}}}{L_{\overline{A'B'}}}, \tag{43}$$

while the circumferential line strain when the circumferential micro-curve element $\overset{\frown}{A'D'}$ becomes the circumferential micro-curve element $\overset{\frown}{AD}$ may be written as (see Figure 16b)

$$e_t = \frac{L_{\overset{\frown}{AD}} - L_{\overset{\frown}{A'D'}}}{L_{\overset{\frown}{A'D'}}}. \tag{44}$$

Obviously, the length of the curve $\overset{\frown}{AB}$ may be approximated by that of the straight line $\overline{AB}$ (see Figure 16a), that is,

$$L_{\overset{\frown}{AB}} \cong L_{\overline{AB}} = \sqrt{(\Delta r + \frac{\mathrm{d}u}{\mathrm{d}r}\Delta r)^2 + (-\frac{\mathrm{d}w}{\mathrm{d}r}\Delta r)^2}. \tag{45}$$

Therefore, the radial line strain e_r may finally be written as

$$e_r = \frac{L_{\overset{\frown}{AB}} - L_{\overline{A'B'}}}{L_{\overline{A'B'}}} = \frac{\sqrt{(\Delta r + \frac{\mathrm{d}u}{\mathrm{d}r}\Delta r)^2 + (-\frac{\mathrm{d}w}{\mathrm{d}r}\Delta r)^2} - \Delta r}{\Delta r} = \sqrt{(1+\frac{\mathrm{d}u}{\mathrm{d}r})^2 + (-\frac{\mathrm{d}w}{\mathrm{d}r})^2} - 1. \tag{46}$$

On the other hand, due to $L_{\overset{\frown}{AD}} = (r+u)\cdot\Delta\varphi$ and $L_{\overset{\frown}{A'D'}} = r\cdot\Delta\varphi$ (see Figure 16b), the circumferential line strain e_t may finally be written as

$$e_t = \frac{L_{\overset{\frown}{AD}} - L_{\overset{\frown}{A'D'}}}{L_{\overset{\frown}{A'D'}}} = \frac{(r+u)\cdot\Delta\varphi - r\cdot\Delta\varphi}{r\cdot\Delta\varphi} = \frac{u}{r}. \tag{47}$$

Equations (46) and (47) are the radial and circumferential geometric equations used in this paper, see Equations (6) and (7) in Section 2.1. However, in the derivation of the classical radial geometric equation, a very inappropriate "assumption", instead of the "approximation" in Equation (45), is used. The classical radial geometric equation is derived as follows. With the assumption of $L_{\overset{\frown}{AB}} = L_{\overline{A'B'}}$, it is found that, from Equation (43)

$$e_r = \frac{L_{\overset{\frown}{AB}} - L_{\overline{A'B'}}}{L_{\overline{A'B'}}} = \frac{(L_{\overset{\frown}{AB}} + L_{\overline{A'B'}})\bullet(L_{\overset{\frown}{AB}} - L_{\overline{A'B'}})}{(L_{\overset{\frown}{AB}} + L_{\overline{A'B'}})\bullet L_{\overline{A'B'}}} = \frac{L^2_{\overset{\frown}{AB}} - L^2_{\overline{A'B'}}}{(L_{\overset{\frown}{AB}} + L_{\overline{A'B'}})\bullet L_{\overline{A'B'}}} \approx \frac{L^2_{\overset{\frown}{AB}} - L^2_{\overline{A'B'}}}{(2L_{\overline{A'B'}})\bullet L_{\overline{A'B'}}} = \frac{L^2_{\overset{\frown}{AB}} - L^2_{\overline{A'B'}}}{2L^2_{\overline{A'B'}}}. \tag{48}$$

After considering Equation (45) and $L_{\overline{A'B'}} = \Delta r$ (see Figure 16a), the classical radial geometric equation is finally written as

$$e_r = \frac{L_{\overset{\frown}{AB}} - L_{\overline{A'B'}}}{L_{\overline{A'B'}}} \approx \frac{L^2_{\overset{\frown}{AB}} - L^2_{\overline{A'B'}}}{2L^2_{\overline{A'B'}}} = \frac{(\Delta r + \frac{\mathrm{d}u}{\mathrm{d}r}\Delta r)^2 + (-\frac{\mathrm{d}w}{\mathrm{d}r}\Delta r)^2 - (\Delta r)^2}{2(\Delta r)^2} = \frac{\mathrm{d}u}{\mathrm{d}r} + \frac{1}{2}(\frac{\mathrm{d}u}{\mathrm{d}r})^2 + \frac{1}{2}(-\frac{\mathrm{d}w}{\mathrm{d}r})^2 \cong \frac{\mathrm{d}u}{\mathrm{d}r} + \frac{1}{2}(-\frac{\mathrm{d}w}{\mathrm{d}r})^2. \tag{49}$$

From the above derivation, it can be concluded that the classical radial geometric equation used in [13], i.e., Equation (6) in [13], or Equation (49) in this paper, only applies to small deflection membranes, and that, no matter how small the deflections, it is essentially invalid, because the adopted assumption of $L_{\overset{\frown}{AB}} = L_{\overline{A'B'}}$ does not hold, even for very small deflections. On the other hand, however, the radial geometric equation used in this paper, i.e., Equation (6) or (46), is not affected by the size of the deflections, because it uses only the "approximation" in Equation (45). It is worth noting that the smaller Δr is, the more accurate Equation (45) is, and the length of the taken radial micro-straight-line element $\overline{A'B'}$, Δr, itself is a quantity that can be as small as expected, because the "micro" here means $\Delta r \to 0$. Therefore, in this sense, the radial geometric equation used in this paper, i.e., Equation (6) or (46), is, in fact, an exact geometric equation for the large deflection problems of thin plates or membranes, while the classical one, i.e., Equation (6) in [13] or Equation (49) in this paper, should be abandoned.

By comparing the governing equations used in Section 2.1 in this paper with those used in Section 2 in [13], it can be seen that only the radial geometric equation is different, while other governing equations, such as the circumferential geometry equation, out-of-plane and in-plane equilibrium equations, and radial and circumferential physical equations, are completely the same. Therefore, the radial geometric equation used in this paper, i.e., Equation (6) or (46), plays a crucial role in improving the performance of the obtained closed-form solutions, in comparison to the classical radial geometric equation used in [13], i.e., Equation (6) in [13], or Equation (49) in this paper. Such an improvement results in a wider range of the nearly-linear segment in the nonlinear *C*-*V* relationship calculated by using the deflection solution obtained in this paper, in comparison with the range calculated by using the deflection solution obtained in [13] (see Figures 12–14). Such a wider range of the nearly-linear segment can be used to develop linear rain gauges; therefore, the closed-form solutions obtained in Section 2 in this paper open up a larger research and development space for linear rain gauges, while the closed-form solutions in [13] should be abandoned.

4.2. Effect of Changes in Elasticity Modulus on Input–Output Relationships

The results of the numerical calculation, which are listed in Table 5 for E = 7.84 MPa, in Table 6 for E = 3.05 MPa, and in Table 7 for E = 1.55 MPa, are used here. The influence of

changing Young's modulus of elasticity E on the relationships of the input capacitance C and output volume V is shown in Figure 17, showing that the degree of linearization of the C-V relationships can be improved by increasing the value of the Young's modulus of elasticity E; in other words, the nonlinearity of the C-V relationships becomes stronger with the decrease of Young's modulus of elasticity E. From Figure 17, it can be observed that the nearly-linear segments in the C-V relationships are about 3–5.6 pF and 18,126,666 mm^3 for E = 7.84 MPa, 3–8 pF and 15,733,468 mm^3 for E = 3.05 MPa, and 3–5.6 pF and 4,911,306 mm^3 for E = 1.55 MPa.

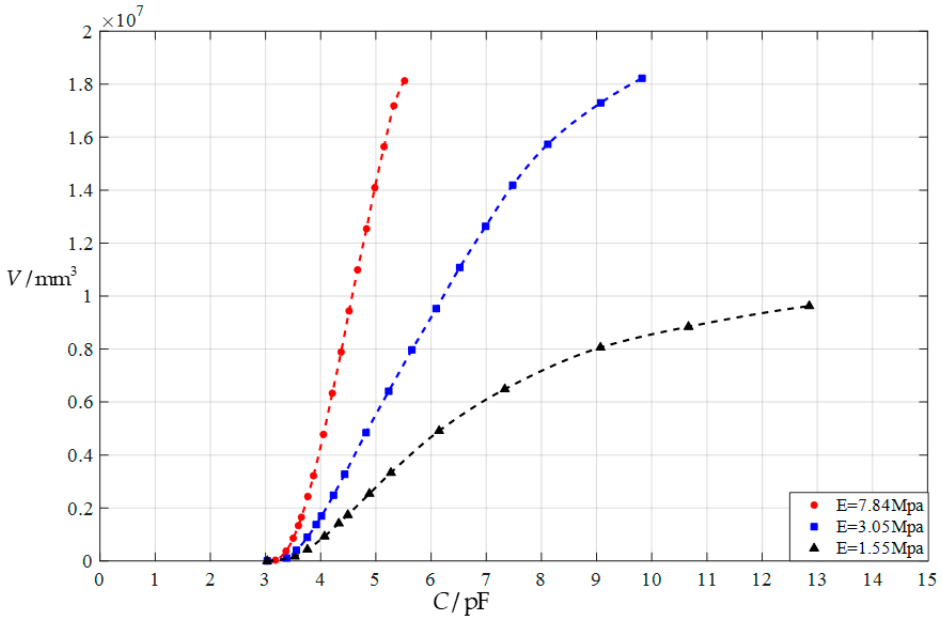

Figure 17. The relationships between the input capacitance C and output volume V, when a = 70 mm, h = 0.3 mm, ν = 0.45, t = 0.1 mm, g = 45 mm, and E = 1.55 MPa, 3.05 MPa, and 7.84 MPa, respectively.

4.3. Effect of Changes in Poisson's Ratio on Input–Output Relationships

In this section, the parameters used in Section 3.2 are still used, except for the Poisson's ratio ν; that is, a = 70 mm, thickness h = 0.3 mm, E = 3.05 MPa, t = 0.1 mm, g = 45 mm, $\varepsilon_0 = 8.854187817 \times 10^{-12}$ F/m, ε_{r1} = 1.0000585, and ε_{r2} = 2.5. Poisson's ratio ν here is 0.35 and 0.25, respectively, in order to compare with the case of using v = 0.45 in Section 3.2. The numerical results calculated by using the deflection solution in Section 2 are listed in Table 11 for v = 0.35, and in Table 12 for v = 0.25, in addition to the results of numerical calculation for v = 0.45, which are listed in Table 6. The influence of changing Poisson's ratio ν on the relationships of the input capacitance C and output volume V is shown in Figure 18, showing that the degree of linearization of the C-V relationships can be improved by increasing the value of Poisson's ratio ν. In other words, the nonlinearity of the C-V relationships becomes stronger with the decrease of Poisson's ratio ν. From Figure 18, it can be observed that the nearly-linear segments of the C-V relationships are about 3–8 pF and 15,733,468 mm^3 for v = 0.45, 3–6.7 pF and 9,547,325 mm^3 for v = 0.35, and 3–6.3 pF and 6,436,267 mm^3 for v = 0.25.

Table 11. The calculation results obtained by using the deflection solution presented in Section 2, when a = 70 mm, h = 0.3 mm, E = 3.05 MPa, ν = 0.35, t = 0.1 mm, and g = 45 mm.

V/mm^3	H/mm	c_0	d_0	σ_m/MPa	w_m/mm	C/pF
0	0	0	0	0	0	3.031
151,249	5	0.01960065	0.13970727	0.060	9.779	3.412
409,891	20	0.03584467	0.18571549	0.109	13.001	3.616
902,358	50	0.05981112	0.23675734	0.182	16.573	3.831

Table 11. *Cont.*

V/mm^3	H/mm	c_0	d_0	σ_m/MPa	w_m/mm	C/pF
1,385,079	80	0.07975804	0.27130274	0.243	18.991	4.045
1,704,436	100	0.09193828	0.29000494	0.280	20.301	4.145
2,498,392	150	0.11995604	0.32807286	0.366	22.965	4.422
3,287,069	200	0.14605552	0.35864799	0.445	25.105	4.650
4,862,035	300	0.19400944	0.40680981	0.592	28.477	5.121
6,428,063	400	0.23822218	0.44559751	0.726	31.192	5.610
7,973,715	500	0.28096429	0.47906534	0.857	33.534	6.106
9,547,325	600	0.32334823	0.50876616	0.982	35.614	6.658
11,103,956	700	0.36364397	0.53606178	1.109	37.524	7.361
12,660,576	800	0.40189638	0.56152032	1.226	39.306	8.287
14,215,831	900	0.44027831	0.58559057	1.343	40.991	9.758
15,652,977	1000	0.47591760	0.61058872	1.4515	42.741	11.896

Table 12. The calculation results obtained by using the deflection solution presented in Section 2, when a = 70 mm, h = 0.3 mm, E = 3.05 MPa, ν = 0.25, t = 0.1 mm, and g = 45 mm.

V/mm^3	H/mm	c_0	d_0	σ_m/MPa	w_m/mm	C/pF
0	0	0	0	0	0	3.031
155,370	5	0.01955022	0.14669016	0.059	10.268	3.436
415,069	20	0.03537019	0.19413305	0.107	13.589	3.694
908,752	50	0.05875659	0.24695086	0.179	17.286	3.966
1,392,544	80	0.07835133	0.28269779	0.239	19.789	4.190
1,712,554	100	0.09031799	0.30215501	0.275	21.151	4.326
2,507,038	150	0.11785215	0.34171298	0.359	23.920	4.651
3,296,568	200	0.14306985	0.37344014	0.436	26.141	4.953
4,869,168	300	0.19031987	0.42400135	0.580	29.680	5.545
6,436,267	400	0.23500158	0.46421485	0.717	32.495	6.251
8,002,575	500	0.27645352	0.50295479	0.843	35.207	7.114
9,560,993	600	0.31807374	0.53012719	0.970	37.109	8.122
11,129,019	700	0.34882488	0.57852073	1.064	40.496	9.503
12,031,455	750	0.37620298	0.58646151	1.147	41.052	10.904
12,702,326	800	0.39534789	0.60851844	1.206	42.596	13.009

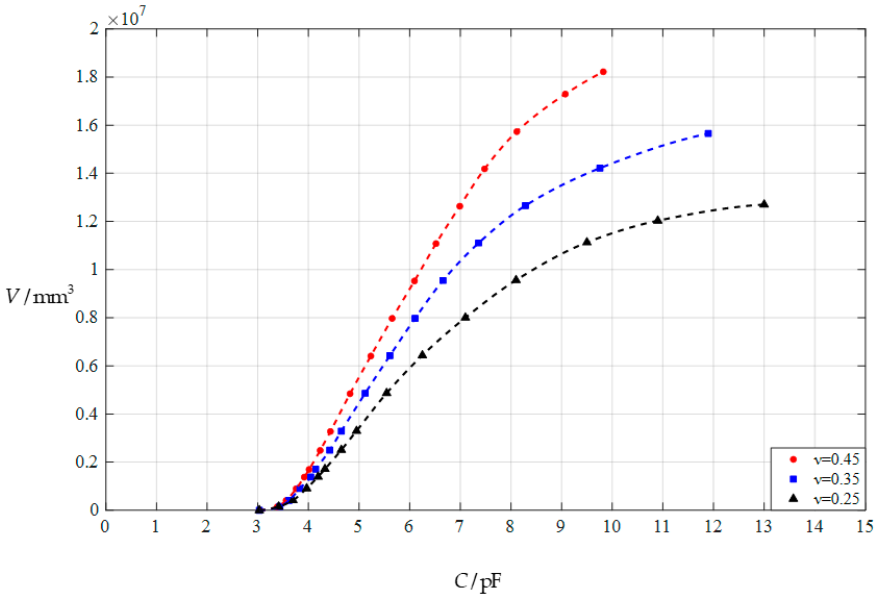

Figure 18. The relationships between the input capacitance C and output volume V, when a = 70 mm, h = 0.3 mm, E = 3.05 MPa, t = 0.1 mm, g = 45 mm, and ν = 0.45, 0.35, and 0.25, respectively.

5. Concluding Remarks

The main contribution of this paper is that by modifying the geometric equations, the differential-integral equations governing the elastic behavior of the deflected membrane were improved, new and more accurate closed-form solutions were presented, and a new and more accurate mathematical theory for designing membrane deflection-based rain gauges was provided. The newly provided mathematical theory can be used to design and numerically calibrate both nonlinear and linear membrane deflection-based rain gauges. From this study, the following conclusions were drawn.

The classical geometric equations are only applicable to small deflection problems due to the use of an inappropriate assumption, while the geometric equations used here abandoned this inappropriate assumption and fully considered the influence of deflection on geometric relationships, and thus apply to the case of arbitrary deflections.

The ranges of the nearly-linear segments in the nonlinear input–output relationships of membrane deflection-based rain gauges, obtained by using the newly presented mathematical theory, were indeed larger or wider than those obtained by using the previously presented mathematical theory. This leads to greater possibilities for developing membrane deflection-based linear rain gauges.

The nonlinear input–output relationships of membrane deflection-based rain gauges can be adjusted by changing some important design parameters, such as Young's modulus of elasticity E and Poisson's ratio ν, which provides a direction for selecting an appropriate conductive circular membrane to meet the range requirements of the input capacitance C and output volume V, when designing linear or nonlinear rain gauges.

The work presented here is still in the stage of theoretical design, and the future works will focus on the dynamic problems that may arise when the conductive circular membrane is loaded by the collected rainwater, as well as the fabrication and experimental calibration of the rain gauges. In short, there may be some potential limitations or challenges that need to be addressed.

Author Contributions: Conceptualization, J.-Y.S.; methodology, N.L. and J.-Y.S.; validation, X.-T.H.; writing—original draft preparation, N.L.; writing—review and editing, N.L. and X.-T.H.; visualization, N.L.; funding acquisition, J.-Y.S. All authors have read and agreed to the published version of the manuscript.

Funding: This research was funded by the National Natural Science Foundation of China (Grant No. 11772072).

Data Availability Statement: Not applicable.

Conflicts of Interest: The authors declare no conflict of interest.

Appendix A

$$d_2 = -\frac{G(d_0+H_0)}{4c_0}$$

$$d_4 = \frac{G^2d_0-32c_0c_2d_2+4G^2d_0^2d_2+G^2H_0+8G^2d_0d_2H_0+4G^2d_2H_0^2}{64c_0^2}$$

$$\begin{aligned}
d_6 = {} & \frac{1}{1152c_0^2d_2}(3G^2d_2^2 - 192c_2^2d_2^2 - 384c_0c_4d_2^2 + 48G^2d_0d_2^3 + 8G^2d_0d_4 - 1536c_0c_2d_2d_4 \\
& +192G^2d_0^2d_2d_4 - 768c_0^2d_4^2 + 48G^2d_2^3H_0 + 8G^2d_4H_0 + 384G^2d_0d_2d_4H_0 + 192G^2d_2d_4H_0^2)
\end{aligned}$$

$$\begin{aligned}
d_8 = {} & \frac{1}{768c_0^2d_2}(-192c_2c_4d_2^2 - 192c_0c_6d_2^2 + 6G^2d_2^4 + 2G^2d_2d_4 - 384c_2^2d_2d_4 - 768c_0c_4d_2d_4 \\
& +112G^2d_0d_2^2d_4 - 768c_0c_2d_4^2 + 96G^2d_0^2d_4^2 + 3G^2d_0d_6 - 1152c_0c_2d_2d_6 + 144G^2d_0^2d_2d_6 \\
& -1152c_0^2d_4d_6 + 112G^2d_2^2d_4H_0 + 192G^2d_0d_4^2H_0 + 3G^2d_6H_0 + 288G^2d_0d_2d_6H_0 + 96G^2d_4^2H_0^2 \\
& +144G^2d_2d_6H_0^2)
\end{aligned}$$

$$\begin{aligned}
d_{10} = {} & \frac{1}{28800c_0^2d_2}(-2880c_4^2d_2^2 - 5760c_2c_6d_2^2 - 5760c_0c_8d_2^2 - 23040c_2c_4d_2d_4 - 23040c_0c_6d_2d_4 \\
& +960G^2d_2^3d_4 + 20G^2d_4^2 - 11520c_2^2d_4^2 - 23040c_0c_4d_4^2 + 4800G^2d_0d_2d_4^2 + 45G^2d_2d_6 - 17280c_2^2d_2d_6 \\
& -34560c_0c_4d_2d_6 + 4680G^2d_0d_2^2d_6 - 69120c_0c_2d_4d_6 + 8640G^2d_0^2d_4d_6 - 25920c_0^2d_6^2 + 72G^2d_0d_8 \\
& -46080c_0c_2d_2d_8 + 5760G^2d_0^2d_2d_8 - 46080c_0^2d_4d_8 + 4800G^2d_2d_4^2H_0 + 4680G^2d_2^2d_6H_0 \\
& +17280G^2d_0d_4d_6H_0 + 72G^2d_8H_0 + 11520G^2d_0d_2d_8H_0 + 8640G^2d_4d_6H_0^2 + 5760G^2d_2d_8H_0^2)
\end{aligned}$$

$$
\begin{aligned}
d_{12} = {} & \tfrac{1}{17280c_0^2d_2}(-2880c_4c_6d_2^2 - 2880c_2c_8d_2^2 - 2880c_0c_{10}d_2^2 - 5760c_4^2d_2d_4 - 11520c_2c_6d_2d_4 \\
& -11520c_0c_8d_2d_4 - 11520c_2c_4d_4^2 - 11520c_0c_6d_4^2 + 880G^2d_2^2d_4^2 + 960G^2d_0d_4^3 - 17280c_2c_4d_2d_6 \\
& -17280c_0c_6d_2d_6 + 630G^2d_2^3d_6 + 15G^2d_4d_6 - 17280c_2^2d_4d_6 - 34560c_0c_4d_4d_6 + 6480G^2d_0d_2d_4d_6 \\
& -25920c_0c_2d_6^2 + 3240G^2d_0^2d_6^2 + 18G^2d_2d_8 - 11520c_2^2d_2d_8 - 23040c_0c_4d_2d_8 + 3024G^2d_0d_2^2d_8 \\
& -46080c_0c_2d_4d_8 + 5760G^2d_0^2d_4d_8 - 34560c_0^2d_6d_8 + 30G^2d_0d_{10} - 28800c_0c_2d_2d_{10} \\
& +3600G^2d_0^2d_2d_{10} - 28800c_0^2d_4d_{10} + 960G^2d_4^3H_0 + 6480G^2d_2d_4d_6H_0 + 6480G^2d_0d_6^2H_0 \\
& +3024G^2d_2^2d_8H_0 + 11520G^2d_0d_4d_8H_0 + 30G^2d_{10}H_0 + 7200G^2d_0d_2d_{10}H_0 + 3240G^2d_6^2H_0^2 \\
& +5760G^2d_4d_8H_0^2 + 3600G^2d_2d_{10}H_0^2) \\
d_{14} = {} & \tfrac{1}{1128960c_0^2d_2}(-80640c_6^2d_2^2 - 161280c_4c_8d_2^2 - 161280c_2c_{10}d_2^2 - 161280c_0c_{12}d_2^2 \\
& -645120c_4c_6d_2d_4 - 645120c_2c_8d_2d_4 - 645120c_0c_{10}d_2d_4 - 322560c_4^2d_4^2 - 645120c_2c_6d_4^2 \\
& -645120c_0c_8d_4^2 + 35840G^2d_2d_4^3 - 483840c_4^2d_2d_6 - 967680c_2c_6d_2d_6 - 967680c_0c_8d_2d_6 \\
& -1935360c_2c_4d_4d_6 - 1935360c_0c_6d_4d_6 + 124320G^2d_2^2d_4d_6 + 201600G^2d_0d_4^2d_6 + 315G^2d_6^2 \\
& -725760c_2^2d_6^2 - 1451520c_0c_4d_6^2 + 241920G^2d_0d_2d_6^2 - 1290240c_2c_4d_2d_8 - 1290240c_0c_6d_2d_8 \\
& +44352G^2d_2^3d_8 + 672G^2d_4d_8 - 1290240c_2^2d_4d_8 - 2580480c_0c_4d_4d_8 + 462336G^2d_0d_2d_4d_8 \\
& -3870720c_0c_2d_6d_8 + 483840G^2d_0^2d_6d_8 - 1290240c_0^2d_8^2 + 840G^2d_2d_{10} - 806400c_2^2d_2d_{10} \\
& -1612800c_0c_4d_2d_{10} + 208320G^2d_0d_2^2d_{10} - 3225600c_0c_2d_4d_{10} + 403200G^2d_0^2d_4d_{10} \\
& -2419200c_0^2d_6d_{10} + 1440G^2d_0d_{12} - 1935360c_0c_2d_2d_{12} + 241920G^2d_0^2d_2d_{12} - 1935360c_0^2d_4d_{12} \\
& +201600G^2d_4^2d_6H_0 + 241920G^2d_2d_6^2H_0 + 462336G^2d_2d_4d_8H_0 + 967680G^2d_0d_6d_8H_0 \\
& +208320G^2d_2^2d_{10}H_0 + 806400G^2d_0d_4d_{10}H_0 + 1440G^2d_{12}H_0 + 483840G^2d_0d_2d_{12}H_0 \\
& +483840G^2d_6d_8H_0^2 + 403200G^2d_4d_{10}H_0^2 + 241920G^2d_2d_{12}H_0^2) \\
d_{16} = {} & \tfrac{1}{322560c_0^2d_2}(-40320c_6c_8d_2^2 - 40320c_4c_{10}d_2^2 - 40320c_2c_{12}d_2^2 - 40320c_0c_{14}d_2^2 \\
& -80640c_6^2d_2d_4 - 161280c_4c_8d_2d_4 - 161280c_2c_{10}d_2d_4 - 161280c_0c_{12}d_2d_4 - 161280c_4c_6d_4^2 \\
& -161280c_2c_8d_4^2 - 161280c_0c_{10}d_4^2 + 2240G^2d_4^4 - 241920c_4c_6d_2d_6 - 241920c_2c_8d_2d_6 \\
& -241920c_0c_{10}d_2d_6 - 241920c_4^2d_4d_6 - 483840c_2c_6d_4d_6 - 483840c_0c_8d_4d_6 + 31920G^2d_2d_4^2d_6 \\
& -362880c_2c_4d_6^2 - 362880c_0c_6d_6^2 + 19215G^2d_2^2d_6^2 + 60480G^2d_0d_4d_6^2 - 161280c_4^2d_2d_8 \\
& -322560c_2c_6d_2d_8 - 322560c_0c_8d_2d_8 - 645120c_2c_4d_4d_8 - 645120c_0c_6d_4d_8 + 38304G^2d_2^2d_4d_8 \\
& +61824G^2d_0d_4^2d_8 + 126G^2d_6d_8 - 483840c_2^2d_6d_8 - 967680c_0c_4d_6d_8 + 153216G^2d_0d_2d_6d_8 \\
& -645120c_0c_2d_8^2 + 80640G^2d_0^2d_8^2 - 403200c_2c_4d_2d_{10} - 403200c_0c_6d_2d_{10} + 13440G^2d_2^3d_{10} \\
& +140G^2d_4d_{10} - 403200c_2^2d_4d_{10} - 806400c_0c_4d_4d_{10} + 141120G^2d_0d_2d_4d_{10} - 1209600c_0c_2d_6d_{10} \\
& +151200G^2d_0^2d_6d_{10} - 806400c_0^2d_8d_{10} + 180G^2d_2d_{12} - 241920c_2^2d_2d_{12} - 483840c_0c_4d_2d_{12} \\
& +61920G^2d_0d_2^2d_{12} - 967680c_0c_2d_4d_{12} + 120960G^2d_0^2d_4d_{12} - 725760c_0^2d_6d_{12} + 315G^2d_0d_{14} \\
& -564480c_0c_2d_2d_{14} + 70560G^2d_0^2d_2d_{14} - 564480c_0^2d_4d_{14} + 60480G^2d_4d_6^2H_0 + 61824G^2d_4^2d_8H_0 \\
& +153216G^2d_2d_6d_8H_0 + 161280G^2d_0d_8^2H_0 + 141120G^2d_2d_4d_{10}H_0 + 302400G^2d_0d_6d_{10}H_0 \\
& +61920G^2d_2^2d_{12}H_0 + 241920G^2d_0d_4d_{12}H_0 + 315G^2d_{14}H_0 + 141120G^2d_0d_2d_{14}H_0 + 80640G^2d_8^2H_0^2 \\
& +151200G^2d_6d_{10}H_0^2 + 120960G^2d_4d_{12}H_0^2 + 70560G^2d_2d_{14}H_0^2) \\
d_{18} = {} & \tfrac{1}{3628800c_0^2d_2}(-201600c_8^2d_2^2 - 403200c_6c_{10}d_2^2 - 403200c_4c_{12}d_2^2 - 403200c_2c_{14}d_2^2 \\
& -403200c_0c_{16}d_2^2 - 1612800c_6c_8d_2d_4 - 1612800c_4c_{10}d_2d_4 - 1612800c_2c_{12}d_2d_4 \\
& -806400c_6^2d_4^2 - 1612800c_4c_8d_4^2 - 1612800c_2c_{10}d_4^2 - 1612800c_0c_{12}d_4^2 - 1209600c_6^2d_2d_6 \\
& -2419200c_4c_8d_2d_6 - 2419200c_2c_{10}d_2d_6 - 2419200c_0c_{12}d_2d_6 - 4838400c_4c_6d_4d_6 \\
& -4838400c_0c_{10}d_4d_6 + 100800G^2d_4^3d_6 - 1814400c_4^2d_6^2 - 3628800c_2c_6d_6^2 - 3628800c_0c_8d_6^2 \\
& +365400G^2d_2d_4d_6^2 + 226800G^2d_0d_6^3 - 3225600c_4c_6d_2d_8 - 3225600c_2c_8d_2d_8 \\
& -3225600c_4^2d_4d_8 - 6451200c_2c_6d_4d_8 - 6451200c_0c_8d_4d_8 + 380800G^2d_2d_4^2d_8 \\
& -9676800c_0c_6d_6d_8 + 468720G^2d_2^2d_6d_8 + 1451520G^2d_0d_4d_6d_8 + 504G^2d_8^2 - 3225600c_2^2d_8^2 \\
& -6451200c_0c_4d_8^2 + 967680G^2d_0d_2d_8^2 - 2016000c_4^2d_2d_{10} - 4032000c_2c_6d_2d_{10} \\
& -8064000c_2c_4d_4d_{10} - 8064000c_0c_6d_4d_{10} + 459200G^2d_2^2d_4d_{10} + 739200G^2d_0d_4^2d_{10} \\
& -6048000c_2^2d_6d_{10} - 12096000c_0c_4d_6d_{10} + 1864800G^2d_0d_2d_6d_{10} - 16128000c_0c_2d_8d_{10} \\
& +2016000G^2d_0^2d_8d_{10} - 5040000c_0^2d_{10}^2 - 4838400c_2c_4d_2d_{12} - 4838400c_0c_6d_2d_{12} \\
& +158400G^2d_2^3d_{12} + 1200G^2d_4d_{12} - 4838400c_2^2d_4d_{12} - 9676800c_0c_4d_4d_{12} \\
& -14515200c_0c_2d_6d_{12} + 1814400G^2d_0^2d_6d_{12} - 9676800c_0^2d_8d_{12} + 1575G^2d_2d_{14} \\
& -5644800c_0c_4d_2d_{14} + 718200G^2d_0d_2^2d_{14} - 11289600c_0c_2d_4d_{14} + 1411200G^2d_0^2d_4d_{14} \\
& +2800G^2d_0d_{16} - 6451200c_0c_2d_2d_{16} + 806400G^2d_0^2d_2d_{16} - 6451200c_0^2d_4d_{16} \\
& +1451520G^2d_4d_6d_8H_0 + 967680G^2d_2d_8^2H_0 + 739200G^2d_4^2d_{10}H_0 + 1864800G^2d_2d_6d_{10}H_0 \\
& +4032000G^2d_0d_8d_{10}H_0 + 1670400G^2d_2d_4d_{12}H_0 + 3628800G^2d_0d_6d_{12}H_0 + \\
& 718200G^2d_2^2d_{14}H_0 + 2822400G^2d_0d_4d_{14}H_0 + 2800G^2d_{16}H_0 + 1612800G^2d_0d_2d_{16}H_0 \\
& -1612800c_0c_{14}d_2d_4 - 4838400c_2c_8d_4d_6 - 3225600c_0c_{10}d_2d_8 - 9676800c_2c_4d_6d_8
\end{aligned}
$$

$$
\begin{aligned}
&-4032000c_0c_8d_2d_{10}+1050G^2d_6d_{10}+1670400G^2d_0d_2d_4d_{12}-2822400c_2^2d_2d_{14}\\
&-8467200c_0^2d_6d_{14}+2016000G^2d_8d_{10}H_0^2+1814400G^2d_6d_{12}H_0^2+1411200G^2d_4d_{14}H_0^2\\
&+226800G^2d_6^3H_0+806400G^2d_2d_{16}H_0^2)\\
d_{20}=&\tfrac{1}{2016000c_0^2d_2}(-201600c_8c_{10}d_2^2-201600c_6c_{12}d_2^2-201600c_4c_{14}d_2^2-201600c_2c_{16}d_2^2\\
&-201600c_0c_{18}d_2^2-403200c_8^2d_2d_4-806400c_6c_{10}d_2d_4-806400c_4c_{12}d_2d_4-806400c_2c_{14}d_2d_4\\
&-806400c_0c_{16}d_2d_4-806400c_6c_8d_4^2-806400c_4c_{10}d_4^2-806400c_2c_{12}d_4^2-806400c_0c_{14}d_4^2\\
&-1209600c_6c_8d_2d_6-1209600c_4c_{10}d_2d_6-1209600c_2c_{12}d_2d_6-1209600c_0c_{14}d_2d_6\\
&-2419200c_4c_8d_4d_6-2419200c_2c_{10}d_4d_6-2419200c_0c_{12}d_4d_6-1814400c_4c_6d_6^2\\
&-1814400c_0c_{10}d_6^2+81900G^2d_4^2d_6^2+66150G^2d_2d_6^3-806400c_6^2d_2d_8-1612800c_4c_8d_2d_8\\
&-1612800c_2c_{10}d_2d_8-1612800c_0c_{12}d_2d_8-3225600c_4c_6d_4d_8-3225600c_2c_8d_4d_8\\
&+58240G^2d_4^3d_8-2419200c_4^2d_6d_8-4838400c_2c_6d_6d_8-4838400c_0c_8d_6d_8\\
&+393120G^2d_0d_6^2d_8-3225600c_2c_4d_8^2-3225600c_0c_6d_8^2+142128G^2d_2^2d_8^2\\
&-2016000c_4c_6d_2d_{10}-2016000c_2c_8d_2d_{10}-2016000c_0c_{10}d_2d_{10}-2016000c_4^2d_4d_{10}\\
&-4032000c_2c_6d_4d_{10}-4032000c_0c_8d_4d_{10}+224000G^2d_2d_4^2d_{10}-6048000c_2c_4d_6d_{10}\\
&-6048000c_0c_6d_6d_{10}+279300G^2d_2^2d_6d_{10}+856800G^2d_0d_4d_6d_{10}+420G^2d_8d_{10}\\
&-4032000c_2^2d_8d_{10}-8064000c_0c_4d_8d_{10}+1176000G^2d_0d_2d_8d_{10}-5040000c_0c_2d_{10}^2\\
&+630000G^2d_0^2d_{10}^2-1209600c_4^2d_2d_{12}-2419200c_2c_6d_2d_{12}-2419200c_0c_8d_2d_{12}\\
&-4838400c_2c_4d_4d_{12}-4838400c_0c_6d_4d_{12}+268800G^2d_2^2d_4d_{12}+432000G^2d_0d_4^2d_{12}\\
&+450G^2d_6d_{12}-3628800c_2^2d_6d_{12}-7257600c_0c_4d_6d_{12}+1101600G^2d_0d_2d_6d_{12}\\
&+1209600G^2d_0^2d_8d_{12}-6048000c_0^2d_{10}d_{12}-2822400c_2c_4d_2d_{14}-2822400c_0c_6d_2d_{14}\\
&+91350G^2d_2^3d_{14}+525G^2d_4d_{14}-2822400c_2^2d_4d_{14}-5644800c_0c_4d_4d_{14}+966000G^2d_0d_2d_4d_{14}\\
&-8467200c_0c_2d_6d_{14}+1058400G^2d_0^2d_6d_{14}-5644800c_0^2d_8d_{14}+700G^2d_2d_{16}-1612800c_2^2d_2d_{16}\\
&-3225600c_0c_4d_2d_{16}+408800G^2d_0d_2^2d_{16}-6451200c_0c_2d_4d_{16}+806400G^2d_0^2d_4d_{16}\\
&-4838400c_0^2d_6d_{16}+1260G^2d_0d_{18}-3628800c_0c_2d_2d_{18}+453600G^2d_0^2d_2d_{18}-3628800c_0^2d_4d_{18}\\
&+393120G^2d_6^2d_8H_0+430080G^2d_4d_8^2H_0+856800G^2d_4d_6d_{10}H_0+1176000G^2d_2d_8d_{10}H_0\\
&+1260000G^2d_0d_{10}^2H_0+432000G^2d_4^2d_{12}H_0+1101600G^2d_2d_6d_{12}H_0+2419200G^2d_0d_8d_{12}H_0\\
&+966000G^2d_2d_4d_{14}H_0+2116800G^2d_0d_6d_{14}H_0+408800G^2d_2^2d_{16}H_0+1612800G^2d_0d_4d_{16}H_0\\
&+1260G^2d_{18}H_0+907200G^2d_0d_2d_{18}H_0+630000G^2d_{10}^2H_0^2+1209600G^2d_8d_{12}H_0^2\\
&-1209600c_6^2d_4d_6-1814400c_2c_8d_6^2-3225600c_0c_{10}d_4d_8+426720G^2d_2d_4d_6d_8\\
&+430080G^2d_0d_4d_8^2-9676800c_0c_2d_8d_{12}+1058400G^2d_6d_{14}H_0^2+806400G^2d_4d_{16}H_0^2\\
&+453600G^2d_2d_{18}H_0^2)
\end{aligned}
$$

Appendix B

$$
\begin{aligned}
c_2=&\tfrac{G^2(H_0+d_0)^2}{64c_0^2(vc_0-c_0-1)}\\
c_4=&\tfrac{4G^2H_0^2d_2^2+8G^2H_0d_0d_2^2+4G^2d_0^2d_2^2-192vc_0^2c_2^2+G^2H_0d_2+G^2d_0d_2+320c_0^2c_2^2-32c_0c_2d_2^2}{192c_0^2(vc_0-c_0-1)}\\
c_6=&\tfrac{1}{4608c_0^2(vc_0-c_0-1)}(192G^2H_0^2d_2d_4+384G^2H_0d_0d_2d_4+48G^2H_0d_2^3+192G^2d_0^2d_2d_4\\
&+48G^2d_0d_2^3-10752vc_0^2c_2c_4+8G^2H_0d_4+8G^2d_0d_4+3G^2d_2^2+21504c_0^2c_2c_4-1536c_0c_2d_2d_4\\
&-384c_0c_4d_2^2-192c_2^2d_2^2)\\
c_8=&\tfrac{1}{3840c_0^2(vc_0-c_0-1)}(144G^2H_0^2d_2d_6+96G^2H_0^2d_4^2+288G^2H_0d_0d_2d_6+192G^2H_0d_0d_4^2\\
&+112G^2H_0d_2^2d_4+144G^2d_0^2d_2d_6+96G^2d_0^2d_4^2+112G^2d_0d_2^2d_4+6G^2d_2^4-9600vc_0^2c_2c_6\\
&-5760vc_0^2c_4^2+3G^2H_0d_6+3G^2d_0d_6+2G^2d_2d_4+21120c_0^2c_2c_6+14976c_0^2c_4^2-1152c_0c_2d_2d_6\\
&-768c_0c_2d_4^2-768c_0c_4d_2d_4-192c_0c_6d_2^2-384c_2^2d_2d_4-192c_2c_4d_2^2)\\
c_{10}=&\tfrac{1}{172800c_0^2(vc_0-c_0-1)}(5760G^2H_0^2d_2d_8+8640G^2H_0^2d_4d_6+11520G^2H_0d_0d_2d_8\\
&+17280G^2H_0d_0d_4d_6+4680G^2H_0d_2^2d_6+4800G^2H_0d_2d_4^2+5760G^2d_0^2d_2d_8+8640G^2d_0^2d_4d_6\\
&+4680G^2d_0d_2^2d_6+4800G^2d_0d_2d_4^2+960G^2d_2^3d_4-449280vc_0^2c_2c_8-587520vc_0^2c_4c_6\\
&+72G^2H_0d_8+72G^2d_0d_8+45G^2d_2d_6+20G^2d_4^2+1048320c_0^2c_2c_8+1762560c_0^2c_4c_6\\
&-46080c_0c_2d_2d_8-69120c_0c_2d_4d_6-34560c_0c_4d_2d_6-23040c_0c_4d_4^2-23040c_0c_6d_2d_4\\
&-5760c_0c_8d_2^2-17280c_2^2d_2d_6-11520c_2^2d_4^2-23040c_2c_4d_2d_4-5760c_2c_6d_2^2-2880c_4^2d_2^2)\\
c_{12}=&\tfrac{1}{120960c_0^2(vc_0-c_0-1)}(3600G^2H_0^2d_2d_{10}+5760G^2H_0^2d_4d_8+3240G^2H_0^2d_6^2+7200G^2H_0d_0d_2d_{10}\\
&+11520G^2H_0d_0d_4d_8+6480G^2H_0d_0d_6^2+3024G^2H_0d_2^2d_8+6480G^2H_0d_2d_4d_6+960G^2H_0d_4^3\\
&+3600G^2d_0^2d_2d_{10}+5760G^2d_0^2d_4d_8+3240G^2d_0^2d_6^2+3024G^2d_0d_2^2d_8+6480G^2d_0d_2d_4d_6+960G^2d_0d_4^3\\
&+630G^2d_2^3d_6+880G^2d_2^2d_4^2-322560vc_0^2c_2c_{10}-443520vc_0^2c_4c_8-241920vc_0^2c_6^2+30G^2H_0d_{10}\\
&+30G^2d_0d_{10}+18G^2d_2d_8+15G^2d_4d_6+783360c_0^2c_2c_{10}+1457280c_0^2c_4c_8+864000c_0^2c_6^2\\
&-28800c_0c_2d_2d_{10}-46080c_0c_2d_4d_8-25920c_0c_2d_6^2-23040c_0c_4d_2d_8-34560c_0c_4d_4d_6-17280c_0c_6d_2d_6\\
&-11520c_0c_6d_4^2-11520c_0c_8d_2d_4-2880c_0c_{10}d_2^2-11520c_2^2d_2d_8-17280c_2^2d_4d_6-17280c_2c_4d_2d_6\\
&-11520c_2c_4d_4^2-11520c_2c_6d_2d_4-2880c_2c_8d_2^2-5760c_4^2d_2d_4-2880c_4c_6d_2^2)
\end{aligned}
$$

$$
\begin{aligned}
c_{14} = {} & \tfrac{1}{9031680c_0{}^2(vc_0-c_0-1)}(241920G^2H_0{}^2d_2d_{12}+403200G^2H_0{}^2d_4d_{10}+483840G^2H_0{}^2d_6d_8\\
& +483840G^2H_0d_0d_2d_{12}+806400G^2H_0d_0d_4d_{10}+967680G^2H_0d_0d_6d_8+208320G^2H_0d_2{}^2d_{10}\\
& +462336G^2H_0d_2d_4d_8+241920G^2H_0d_2d_6{}^2+201600G^2H_0d_4{}^2d_6+241920G^2d_0{}^2d_2d_{12}\\
& +403200G^2d_0{}^2d_4d_{10}+483840G^2d_0{}^2d_6d_8+208320G^2d_0d_2{}^2d_{10}+462336G^2d_0d_2d_4d_8\\
& +241920G^2d_0d_2d_6{}^2+201600G^2d_0d_4{}^2d_6+44352G^2d_2{}^3d_8+124320G^2d_2{}^2d_4d_6\\
& +35840G^2d_2d_4{}^3-24514560vc_0{}^2c_2c_{12}-34836480vc_0{}^2c_4c_{10}-39997440vc_0{}^2c_6c_8+1440G^2H_0d_{12}\\
& +1440G^2d_0d_{12}+840G^2d_2d_{10}+672G^2d_4d_8+315G^2d_6{}^2+61286400c_0{}^2c_2c_{12}+121927680c_0{}^2c_4c_{10}\\
& +159989760c_0{}^2c_6c_8-1935360c_0c_2d_2d_{12}-3225600c_0c_2d_4d_{10}-3870720c_0c_2d_6d_8\\
& -1612800c_0c_4d_2d_{10}-2580480c_0c_4d_4d_8-1451520c_0c_4d_6{}^2-1290240c_0c_6d_2d_8-1935360c_0c_6d_4d_6\\
& -967680c_0c_8d_2d_6-645120c_0c_8d_4{}^2-645120c_0c_{10}d_2d_4-161280c_0c_{12}d_2{}^2-806400c_2{}^2d_2d_{10}\\
& -1290240c_2{}^2d_4d_8-725760c_2{}^2d_6{}^2-1290240c_2c_4d_2d_8-1935360c_2c_4d_4d_6-967680c_2c_6d_2d_6\\
& -645120c_2c_6d_4{}^2-645120c_2c_8d_2d_4-161280c_2c_{10}d_2{}^2-483840c_4{}^2d_2d_6-322560c_4{}^2d_4{}^2\\
& -645120c_4c_6d_2d_4-161280c_4c_8d_2{}^2-80640c_6{}^2d_2{}^2)\\
c_{16} = {} & \tfrac{1}{2903040c_0{}^2(vc_0-c_0-1)}(70560G^2H_0{}^2d_2d_{14}+120960G^2H_0{}^2d_4d_{12}+151200G^2H_0{}^2d_6d_{10}\\
& +80640G^2H_0{}^2d_8{}^2+141120G^2H_0d_0d_2d_{14}+241920G^2H_0d_0d_4d_{12}+302400G^2H_0d_0d_6d_{10}\\
& +161280G^2H_0d_0d_8{}^2+61920G^2H_0d_2{}^2d_{12}+141120G^2H_0d_2d_4d_{10}+153216G^2H_0d_2d_6d_8\\
& +61824G^2H_0d_4{}^2d_8+60480G^2H_0d_4d_6{}^2+70560G^2d_0{}^2d_2d_{14}+120960G^2d_0{}^2d_4d_{12}+151200G^2d_0{}^2d_6d_{10}\\
& +80640G^2d_0{}^2d_8{}^2+61920G^2d_0d_2{}^2d_{12}+141120G^2d_0d_2d_4d_{10}+153216G^2d_0d_2d_6d_8+61824G^2d_0d_4{}^2d_8\\
& +60480G^2d_0d_4d_6{}^2+13440G^2d_2{}^3d_{10}+38304G^2d_2{}^2d_4d_8+19215G^2d_2{}^2d_6{}^2+31920G^2d_2d_4{}^2d_6\\
& +2240G^2d_4{}^4-7983360vc_0{}^2c_2c_{14}-11612160vc_0{}^2c_4c_{12}-13789440vc_0{}^2c_6c_{10}-7257600vc_0{}^2c_8{}^2\\
& +315G^2H_0d_{14}+315G^2d_0d_{14}+180G^2d_2d_{12}+140G^2d_4d_{10}+126G^2d_6d_8+20401920c_0{}^2c_2c_{14}\\
& +42577920c_0{}^2c_4c_{12}+59754240c_0{}^2c_6c_{10}+33062400c_0{}^2c_8{}^2-564480c_0c_2d_2d_{14}-967680c_0c_2d_4d_{12}\\
& -1209600c_0c_2d_6d_{10}-645120c_0c_2d_8{}^2-483840c_0c_4d_2d_{12}-806400c_0c_4d_4d_{10}-967680c_0c_4d_6d_8\\
& -403200c_0c_6d_2d_{10}-645120c_0c_6d_4d_8-362880c_0c_6d_6{}^2-322560c_0c_8d_2d_8-483840c_0c_8d_4d_6\\
& -241920c_0c_{10}d_2d_6-161280c_0c_{10}d_4{}^2-161280c_0c_{12}d_2d_4-40320c_0c_{14}d_2{}^2-241920c_2{}^2d_2d_{12}\\
& -403200c_2{}^2d_4d_{10}-483840c_2{}^2d_6d_8-403200c_2c_4d_2d_{10}-645120c_2c_4d_4d_8-362880c_2c_4d_6{}^2\\
& -322560c_2c_6d_2d_8-483840c_2c_6d_4d_6-241920c_2c_8d_2d_6-161280c_2c_8d_4{}^2-161280c_2c_{10}d_2d_4\\
& -40320c_2c_{12}d_2{}^2-161280c_4{}^2d_2d_8-241920c_4{}^2d_4d_6-241920c_4c_6d_2d_6-161280c_4c_6d_4{}^2-161280c_4c_8d_2d_4\\
& -40320c_4c_{10}d_2{}^2-80640c_6{}^2d_2d_4-40320c_6c_8d_2{}^2)\\
c_{18} = {} & \tfrac{1}{36288000c_0{}^2(vc_0-c_0-1)}(806400G^2H_0{}^2d_2d_{16}+1411200G^2H_0{}^2d_4d_{14}+1814400G^2H_0{}^2d_6d_{12}\\
& +2016000G^2H_0{}^2d_8d_{10}+1612800G^2H_0d_0d_2d_{16}+2822400G^2H_0d_0d_4d_{14}+3628800G^2H_0d_0d_6d_{12}\\
& +4032000G^2H_0d_0d_8d_{10}+718200G^2H_0d_2{}^2d_{14}+1670400G^2H_0d_2d_4d_{12}+1864800G^2H_0d_2d_6d_{10}\\
& +967680G^2H_0d_2d_8{}^2+739200G^2H_0d_4{}^2d_{10}+1451520G^2H_0d_4d_6d_8+226800G^2H_0d_6{}^3\\
& +806400G^2d_0{}^2d_2d_{16}+1411200G^2d_0{}^2d_4d_{14}+1814400G^2d_0{}^2d_6d_{12}+2016000G^2d_0{}^2d_8d_{10}\\
& +718200G^2d_0d_2{}^2d_{14}+1670400G^2d_0d_2d_4d_{12}+1864800G^2d_0d_2d_6d_{10}+967680G^2d_0d_2d_8{}^2\\
& +739200G^2d_0d_4{}^2d_{10}+1451520G^2d_0d_4d_6d_8+226800G^2d_0d_6{}^3+158400G^2d_2{}^3d_{12}+459200G^2d_2{}^2d_4d_{10}\\
& +468720G^2d_2{}^2d_6d_8+380800G^2d_2d_4{}^2d_8+365400G^2d_2d_4d_6{}^2+100800G^2d_4{}^3d_6-100800000vc_0{}^2c_2c_{16}\\
& -149184000vc_0{}^2c_4c_{14}-181440000vc_0{}^2c_6c_{12}-197568000vc_0{}^2c_8c_{10}+2800G^2H_0d_{16}+2800G^2d_0d_{16}\\
& +1575G^2d_2d_{14}+1200G^2d_4d_{12}+1050G^2d_6d_{10}+504G^2d_8{}^2+262080000c_0{}^2c_2c_{16}+566899200c_0{}^2c_4c_{14}\\
& +834624000c_0{}^2c_6c_{12}+987840000c_0{}^2c_8c_{10}-6451200c_0c_2d_2d_{16}-11289600c_0c_2d_4d_{14}\\
& -14515200c_0c_2d_6d_{12}-16128000c_0c_2d_8d_{10}-5644800c_0c_4d_2d_{14}-9676800c_0c_4d_4d_{12}\\
& -12096000c_0c_4d_6d_{10}-6451200c_0c_4d_8{}^2-4838400c_0c_6d_2d_{12}-8064000c_0c_6d_4d_{10}-9676800c_0c_6d_6d_8\\
& -4032000c_0c_8d_2d_{10}-6451200c_0c_8d_4d_8-3628800c_0c_8d_6{}^2-3225600c_0c_{10}d_2d_8-4838400c_0c_{10}d_4d_6\\
& -2419200c_0c_{12}d_2d_6-1612800c_0c_{12}d_4{}^2-1612800c_0c_{14}d_2d_4-403200c_0c_{16}d_2{}^2-2822400c_2{}^2d_2d_{14}\\
& -4838400c_2{}^2d_4d_{12}-6048000c_2{}^2d_6d_{10}-3225600c_2{}^2d_8{}^2-4838400c_2c_4d_2d_{12}-8064000c_2c_4d_4d_{10}\\
& -9676800c_2c_4d_6d_8-4032000c_2c_6d_2d_{10}-6451200c_2c_6d_4d_8-3628800c_2c_6d_6{}^2-3225600c_2c_8d_2d_8\\
& -4838400c_2c_8d_4d_6-2419200c_2c_{10}d_2d_6-1612800c_2c_{10}d_4{}^2-1612800c_2c_{12}d_2d_4-403200c_2c_{14}d_2{}^2\\
& -2016000c_4{}^2d_2d_{10}-3225600c_4{}^2d_4d_8-1814400c_4{}^2d_6{}^2-3225600c_4c_6d_2d_8-4838400c_4c_6d_4d_6\\
& -2419200c_4c_8d_2d_6-1612800c_4c_8d_4{}^2-1612800c_4c_{10}d_2d_4-403200c_4c_{12}d_2{}^2-1209600c_6{}^2d_2d_6\\
& -806400c_6{}^2d_4{}^2-1612800c_6c_8d_2d_4-403200c_6c_{10}d_2{}^2-201600c_8{}^2d_2{}^2)\\
c_{20} = {} & \tfrac{1}{22176000c_0{}^2(vc_0-c_0-1)}(453600G^2H_0{}^2d_2d_{18}+806400G^2H_0{}^2d_4d_{16}+1058400G^2H_0{}^2d_6d_{14}\\
& +1209600G^2H_0{}^2d_8d_{12}+630000G^2H_0{}^2d_{10}{}^2+907200G^2H_0d_0d_2d_{18}+1612800G^2H_0d_0d_4d_{16}\\
& +2116800G^2H_0d_0d_6d_{14}+2419200G^2H_0d_0d_8d_{12}+1260000G^2H_0d_0d_{10}{}^2+408800G^2H_0d_2{}^2d_{16}\\
& +966000G^2H_0d_2d_4d_{14}+1101600G^2H_0d_2d_6d_{12}+1176000G^2H_0d_2d_8d_{10}+432000G^2H_0d_4{}^2d_{12}\\
& +856800G^2H_0d_4d_6d_{10}+430080G^2H_0d_4d_8{}^2+393120G^2H_0d_6{}^2d_8+453600G^2d_0{}^2d_2d_{18}\\
& +806400G^2d_0{}^2d_4d_{16}+1058400G^2d_0{}^2d_6d_{14}+1209600G^2d_0{}^2d_8d_{12}+630000G^2d_0{}^2d_{10}{}^2\\
& +408800G^2d_0d_2{}^2d_{16}+966000G^2d_0d_2d_4d_{14}+1101600G^2d_0d_2d_6d_{12}+1176000G^2d_0d_2d_8d_{10}\\
& +432000G^2d_0d_4{}^2d_{12}+856800G^2d_0d_4d_6d_{10}+430080G^2d_0d_4d_8{}^2+393120G^2d_0d_6{}^2d_8+91350G^2d_2{}^3d_{14}\\
& +268800G^2d_2{}^2d_4d_{12}+279300G^2d_2{}^2d_6d_{10}+142128G^2d_2{}^2d_8{}^2+224000G^2d_2d_4{}^2d_{10}+426720G^2d_2d_4d_6d_8\\
& +66150G^2d_2d_6{}^3+58240G^2d_4{}^3d_8+81900G^2d_4{}^2d_6{}^2-62092800vc_0{}^2c_2c_{18}-93139200vc_0{}^2c_4c_{16}\\
& -115315200vc_0{}^2c_6c_{14}-128620800vc_0{}^2c_8c_{12}-66528000vc_0{}^2c_{10}{}^2+1260G^2H_0d_{18}+1260G^2d_0d_{18}\\
& +700G^2d_2d_{16}+525G^2d_4d_{14}+450G^2d_6d_{12}+420G^2d_8d_{10}+163699200c_0{}^2c_2c_{18}+364089600c_0{}^2c_4c_{16}\\
& +555609600c_0{}^2c_6c_{14}+689875200c_0{}^2c_8c_{12}+368928000c_0{}^2c_{10}{}^2-3628800c_0c_2d_2d_{18}-6451200c_0c_2d_4d_{16}\\
& -8467200c_0c_2d_6d_{14}-9676800c_0c_2d_8d_{12}-5040000c_0c_2d_{10}{}^2-3225600c_0c_4d_2d_{16}-5644800c_0c_4d_4d_{14}\\
& -7257600c_0c_4d_6d_{12}-8064000c_0c_4d_8d_{10}-2822400c_0c_6d_2d_{14}-4838400c_0c_6d_4d_{12}-6048000c_0c_6d_6d_{10}\\
& -3225600c_0c_6d_8{}^2-2419200c_0c_8d_2d_{12}-4032000c_0c_8d_4d_{10}-4838400c_0c_8d_6d_8-2016000c_0c_{10}d_2d_{10}
\end{aligned}
$$

$$-3225600c_0c_{10}d_4d_8 - 1814400c_0c_{10}{d_6}^2 - 1612800c_0c_{12}d_2d_8 - 2419200c_0c_{12}d_4d_6 - 1209600c_0c_{14}d_2d_6$$
$$-806400c_0c_{14}{d_4}^2 - 806400c_0c_{16}d_2d_4 - 201600c_0c_{18}{d_2}^2 - 1612800{c_2}^2d_2d_{16} - 2822400{c_2}^2d_4d_{14}$$
$$-3628800{c_2}^2d_6d_{12} - 4032000{c_2}^2d_8d_{10} - 2822400c_2c_4d_2d_{14} - 4838400c_2c_4d_4d_{12} - 6048000c_2c_4d_6d_{10}$$
$$-3225600c_2c_4{d_8}^2 - 2419200c_2c_6d_2d_{12} - 4032000c_2c_6d_4d_{10} - 4838400c_2c_6d_6d_8 - 2016000c_2c_8d_2d_{10}$$
$$-3225600c_2c_8d_4d_8 - 1814400c_2c_8{d_6}^2 - 1612800c_2c_{10}d_2d_8 - 2419200c_2c_{10}d_4d_6 - 1209600c_2c_{12}d_2d_6$$
$$-806400c_2c_{12}{d_4}^2 - 806400c_2c_{14}d_2d_4 - 201600c_2c_{16}{d_2}^2 - 1209600{c_4}^2d_2d_{12} - 2016000{c_4}^2d_4d_{10}$$
$$-2419200{c_4}^2d_6d_8 - 2016000c_4c_6d_2d_{10} - 3225600c_4c_6d_4d_8 - 1814400c_4c_6{d_6}^2 - 1612800c_4c_8d_2d_8$$
$$-2419200c_4c_8d_4d_6 - 1209600c_4c_{10}d_2d_6 - 806400c_4c_{10}{d_4}^2 - 806400c_4c_{12}d_2d_4 - 201600c_4c_{14}{d_2}^2$$
$$-806400{c_6}^2d_2d_8 - 1209600{c_6}^2d_4d_6 - 1209600c_6c_8d_2d_6 - 806400c_6c_8{d_4}^2 - 806400c_6c_{10}d_2d_4$$
$$-201600c_6c_{12}{d_2}^2 - 403200{c_8}^2d_2d_4 - 201600c_8c_{10}{d_2}^2)$$

References

1. Zhang, C.H.; Fan, L.J.; Tan, Y.F. Sequential limit analysis for clamped circular membranes involving large deformation subjected to pressure load. *Int. J. Mech. Sci.* **2019**, *155*, 440–449. [CrossRef]
2. Li, X.; Sun, J.-Y.; Lu, X.-C.; Yang, Z.-X.; He, X.-T. Steady fluid–structure coupling interface of circular membrane under liquid weight loading: Closed-form solution for differential-integral equations. *Mathematics* **2021**, *9*, 1105. [CrossRef]
3. Bernardo, P.; Iulianelli, A.; Macedonio, F.; Drioli, E. Membrane technologies for space engineering. *J. Membr. Sci.* **2021**, *626*, 119177. [CrossRef]
4. Ma, Y.; Wang, G.R.; Chen, Y.L.; Long, D.; Guan, Y.C.; Liu, L.Q.; Zhang, Z. Extended Hencky solution for the blister test of nanomembrane. *Extrem. Mech. Lett.* **2018**, *22*, 69–78. [CrossRef]
5. Dai, Z.; Lu, N. Poking and bulging of suspended thin sheets: Slippage, instabilities, and metrology. *J. Mech. Phys. Solids* **2021**, *149*, 104320. [CrossRef]
6. Tai, Y.; Zhou, K.; Chen, N. Dynamic Properties of Microresonators with the Bionic Structure of Tympanic Membrane. *Sensors* **2020**, *20*, 6958. [CrossRef]
7. Lian, Y.-S.; Sun, J.-Y.; Zhao, Z.-H.; Li, S.-Z.; Zheng, Z.-L. A refined theory for characterizing adhesion of elastic coatings on rigid substrates based on pressurized blister test methods: Closed-form solution and energy release rate. *Polymers* **2020**, *12*, 1788. [CrossRef]
8. Li, X.; Sun, J.-Y.; Shi, B.-B.; Zhao, Z.-H.; He, X.-T. A theoretical study on an elastic polymer thin film-based capacitive wind-pressure sensor. *Polymers* **2020**, *12*, 2133. [CrossRef] [PubMed]
9. Jindal, S.K.; Varma, M.A.; Thukral, D. Comprehensive assessment of MEMS double touch mode capacitive pressure sensor on utilization of SiC film as primary sensing element: Mathematical modelling and numerical simulation. *Microelectron. J.* **2018**, *73*, 30–36. [CrossRef]
10. Lee, H.Y.; Choi, B. Theoretical and experimental investigation of the trapped air effect on air-sealed capacitive pressure sensor. *Sens. Actuat. A-Phys.* **2015**, *221*, 104–114. [CrossRef]
11. Jindal, S.K.; Mahajan, A.; Raghuwanshi, S.K. A complete analytical model for clamped edge circular diaphragm non-touch and touch mode capacitive pressure sensor. *Microsyst. Technol.* **2016**, *22*, 1143–1150. [CrossRef]
12. Li, F.-Y.; Zhang, Q.; Li, X.; He, X.-T.; Sun, J.-Y. Polymer conductive membrane-based non-touch mode circular capacitive pressure sensors: An analytical solution-based method for design and numerical calibration. *Polymers* **2022**, *14*, 3087. [CrossRef]
13. Sun, J.-Y.; Zhang, Q.; Wu, J.; Li, X.; He, X.-T. Large Deflection Analysis of Peripherally Fixed Circular Membranes Subjected to Liquid Weight Loading: A Refined Design Theory of Membrane Deflection-Based Rain Gauges. *Materials* **2021**, *14*, 1023. [CrossRef]
14. Humphrey, M.D.; Istok, J.D.; Lee, J.Y.; Hevesi, J.A.; Flint, A.L. A new method for automated dynamic calibration of tipping-bucket rain gauges. *J. Atmos. Ocean. Technol.* **1997**, *14*, 1513–1519. [CrossRef]
15. Habib, E.; Krajewski, W.F.; Kruger, A. Sampling errors of tipping-bucket rain gauge measurements. *J. Hydrol. Eng.* **2001**, *6*, 159–166. [CrossRef]
16. Molini, A.; Lanza, L.G.; La Barbera, P. Improving the accuracy of tipping-bucket rain records using disaggregation techniques. *Atmos. Res.* **2005**, *77*, 203–217. [CrossRef]
17. Vasvári, V. Calibration of tipping bucket rain gauges in the Graz urban research area. *Atmos. Res.* **2005**, *77*, 18–28. [CrossRef]
18. Habib, E.; Meselhe, E.A.; Aduvala, A.V. Effect of local errors of tipping-bucket rain gauges on rainfall-runoff simulations. *J. Hydrol. Eng.* **2008**, *13*, 488–496. [CrossRef]
19. Colli, M.; Lanza, L.G.; La Barbera, P. Performance of a weighing rain gauge under laboratory simulated time-varying reference rainfall rates. *Atmos. Res.* **2013**, *131*, 3–12. [CrossRef]
20. Colli, M.; Lanza, L.G.; La Barbera, P.; Chan, P.W. Measurement accuracy of weighing and tipping-bucket rainfall intensity gauges under dynamic laboratory testing. *Atmos. Res.* **2014**, *144*, 186–194. [CrossRef]
21. Colli, M.; Lanza, L.G.; Chan, P.W. Co-located tipping-bucket and optical drop counter RI measurements and a simulated correction algorithm. *Atmos. Res.* **2013**, *119*, 3–12. [CrossRef]
22. Bin Afzal, M.H. Effective application of optical sensing technology for sustainable liquid level sensing and rainfall measurement. In *Optical Sensors*; SPIE: Bellingham, DC, USA, 2015; p. 9506.
23. Borup, M.; Grum, M.; Linde, J.J.; Mikkelsen, P.S. Dynamic gauge adjustment of high-resolution X-band radar data for convective rain storms: Model-based evaluation against measured combined sewer overflow. *J. Hydrol.* **2016**, *539*, 687–699. [CrossRef]

24. Bergmann, H.; Breinhllter, H.; Hahle, O.; Krainer, R. Calibration of tipping bucket hyetographs. *Phys. Chem. Earth (C)* **2001**, *26*, 731–736. [CrossRef]
25. Segovia-Cardozo, D.A.; Rodriguez-Sinobas, L.; Diez-Herrero, A.; Zubelzu, S.; Canales-Ide, F. Understanding the Mechanical Biases of Tipping-Bucket Rain Gauges: A Semi-Analytical Calibration Approach. *Water* **2021**, *13*, 2285. [CrossRef]
26. Liao, M.; Liao, A.; Liu, J.; Cai, Z.; Liu, H.; Ma, T. A novel method and system for the fast calibration of tipping bucket rain gauges. *J. Hydrol.* **2021**, *597*, 125782. [CrossRef]
27. Schwamback, D.; Anache, J.A.A.; Wendland, E.C. Calibration and error investigation of large tipping bucket flow meters. *Catena* **2022**, *209*, 105834. [CrossRef]
28. Sevruk, B. Adjustment of tipping-bucket precipitation gauge measurements. *Atmos. Res.* **1996**, *42*, 237–246. [CrossRef]
29. Fankhauser, R. Influence of systematic errors from tipping bucket rain gauges on recorded rainfall data. *Water Sci. Technol.* **1998**, *37*, 121–129. [CrossRef]
30. Shedekar, V.S.; King, K.W.; Fausey, N.R.; Soboyejo, A.B.O.; Harmel, R.D.; Brown, L.C. Assessment of measurement errors and dynamic calibration methods for three different tipping bucket rain gauges. *Atmos. Res.* **2016**, *178*, 445–458. [CrossRef]
31. Sypka, P. Dynamic real-time volumetric correction for tipping-bucket rain gauges. *Agric. For. Meteorol.* **2019**, *271*, 158–167. [CrossRef]
32. Hoffmann, M.; Schwartengräber, R.; Wessolek, G.; Peters, A. Comparison of simple rain gauge measurements with precision lysimeter data. *Atmos. Res.* **2016**, *174*, 120–123. [CrossRef]
33. Lian, Y.-S.; Sun, J.-Y.; Yang, Z.-X.; He, X.-T.; Zheng, Z.-L. Closed-form solution of well-known Hencky problem without small-rotation-angle assumption. *Z. Angew. Math. Mech.* **2016**, *96*, 1434–1441. [CrossRef]
34. Lian, Y.-S.; Sun, J.-Y.; Zhao, Z.-H.; He, X.-T.; Zheng, Z.-L. A revisit of the boundary value problem for Föppl–Hencky membranes: Improvement of geometric equations. *Mathematics* **2020**, *8*, 631. [CrossRef]
35. Moghadam, R.A.; Ebrahimi, S. Design and Analysis of a Torsional Mode MEMS Disk Resonator for RF Applications. *J. Multidiscip. Eng. Sci. Technol.* **2021**, *8*, 14300–14303.
36. Mojtahedi, A.; Hokmabady, H.; Kouhi, M.; Mohammadyzadeh, S. A novel ANN-RDT approach for damage detection of a composite panel employing contact and non-contact measuring data. *Compos. Struct.* **2022**, *279*, 114794. [CrossRef]
37. Ghasemvand, M.; Behjat, B.; Ebrahimi, S. Experimental investigation of the effects of adhesive defects on the strength and creep behavior of single-lap adhesive joints at various temperatures. *J. Adhes.* **2023**, *99*, 1227–1243. [CrossRef]
38. Ahmadi, Z.; Haghighi, M.; Validi, Z. A Novel Approach for Energy Optimization in Distributed Databases in Wireless Network Applications. *J. Manag. Account. Stud.* **2020**, *8*, 50–55. [CrossRef]
39. Velidi, G. Pressure and Velocity Variation in Remote-Controlled Plane Using CFD Analysis. *J. Airl. Oper. Aviat. Manag.* **2022**, *1*, 9–18. [CrossRef]
40. Bhosale, A.; Patil, S.; Dhepe, V.; Banosde, K.; Kakde, R.; Teltumade, R.; Lengare, D. 3-D Numerical Study of Effect of Urea Injector Location and Intake Cone Geometry on SCR Performance. *Int. J. Innov. Res. Sci. Stud.* **2022**, *5*, 47–58. [CrossRef]
41. Moghaddam, B.P.; Tenreiro Machado, J.A. A computational approach for the solution of a class of variable-order fractional integro-differential equations with weakly singular kernels. *Fract. Calc. Appl. Anal.* **2017**, *20*, 1023–1042. [CrossRef]
42. Mokhtary, P.; Moghaddam, B.P.; Lopes, A.M.; Tenreiro Machado, J.A. A computational approach for the non-smooth solution of non-linear weakly singular Volterra integral equation with proportional delay. *Numer. Algorithms* **2020**, *83*, 987–1006. [CrossRef]

Disclaimer/Publisher's Note: The statements, opinions and data contained in all publications are solely those of the individual author(s) and contributor(s) and not of MDPI and/or the editor(s). MDPI and/or the editor(s) disclaim responsibility for any injury to people or property resulting from any ideas, methods, instructions or products referred to in the content.